University of Central Florida
STARS

Electronic Theses and Dissertations

2006

A Methodology For Instrumented Indentation Studies Of Deformation In Bulk Metallic Glasses

Subhaashree Sridharan
University of Central Florida

 Part of the Materials Science and Engineering Commons
Find similar works at: https://stars.library.ucf.edu/etd
University of Central Florida Libraries http://library.ucf.edu

This Masters Thesis (Open Access) is brought to you for free and open access by STARS. It has been accepted for inclusion in Electronic Theses and Dissertations by an authorized administrator of STARS. For more information, please contact STARS@ucf.edu.

STARS Citation
Sridharan, Subhaashree, "A Methodology For Instrumented Indentation Studies Of Deformation In Bulk Metallic Glasses" (2006). *Electronic Theses and Dissertations*. 858.
https://stars.library.ucf.edu/etd/858

A METHODOLOGY FOR INSTRUMENTED INDENTATION STUDIES OF DEFORMATION IN BULK METALLIC GLASSES

by

SUBHAASHREE SRIDHARAN
B.S. Math, University of Madras, Madras, 1999
M.S. Math, Indian Institute of Technology, Madras, 2001

A thesis submitted in partial fulfillment of the requirements
for the degree of Master of Science
in the Department of Mechanical, Materials, and Aerospace Engineering
in the College of Engineering and Computer Science
at the University of Central Florida
Orlando, Florida

Fall Term
2006

Major Professor: Raj Vaidyanathan

ABSTRACT

Bulk Metallic Glasses (BMGs), also known as amorphous metals, are of considerable scientific and commercial interest due to their random or chaotic structure. Given their potential use as engineering materials, there is a concomitant need to establish their mechanical properties. However, BMGs are not conveniently available in sufficient volumes (especially experimental and combinatorial compositions), making property determination via conventional tensile or compression testing problematic. Instrumented indentation is ideally suited for this purpose because the testing requires only small sampling volumes and can probe multiaxial deformation characteristics at various length scales. In this technique, conducted generally on a sub-micron regime, the depth of penetration of an indenter, usually a diamond, is measured as a function of the applied load and expressed graphically as load (P) - displacement (h) curves from which a host of mechanical properties can be extracted and studied.

In this work, a methodology for using instrumented indentation at nano- and micro-scales to determine the mechanical response of BMGs was developed and implemented. The implementation primarily focused on deformation in the elastic regime but included preliminary results related to the onset of inelastic deformation. The methodology developed included calibration techniques, formulations to extract the machine compliances, verifications using standards and verification for uniqueness of instrument deformation under a spherical indenter. The methodology was different for the two platforms used based on the load-depth response characteristics of the instrument. In the case of the Micro Test platform, the load-depth response of the instrument was linear. In the case of the Nano Test platform, the

instrument load-depth response followed a 3/2 power law, representative of Hertzian behavior. The load-depth response of the instrument was determined by subtracting the theoretical response from the corresponding raw load-depth response obtained by elastically indenting a standard steel specimen of known modulus. The true response of the sample was then obtained by subtracting the instrument's response from the corresponding uncorrected load-depth response (raw data). An analytical model to describe the load-train compliance was developed. The methodology was verified using quartz and tungsten standards.

Indentation experiments were conducted on $Zr_{41.25}Ti_{13.75}Cu_{12.5}Ni_{10}Be_{22.5}$ (Vitreloy 1), $Cu_{60}Hf_{25}Ti_{15}$, $Cu_{60}Zr_{30}Ti_{10}$ and $Fe_{60}Co_7Zr_{10}Mo_5W_2B_{16}$ bulk metallic glasses using spherical indenters with diameters 2.8 mm and 100 μm. The spherical geometry results in a simpler stress distribution under the indenter (when compared to a sharp geometry) and furthermore by recourse to spherical indenters the onset of plastic deformation was delayed.

In the case of the Zr-based BMG, the experiments showed that the elastic response did not depend on the diameter of the indenter used indicative of the absence of residual stresses in the sample. Large scale plastic deformation was observed when the sample was indented using a smaller diameter indenter. Log scale analysis (i.e., examining the results on a log load vs. log depth response to check for deviation from Hertzian behavior) showed a deviation from a 3/2 fit indicating a deviation from elastic behavior. The onset implied a yield strength value of ~ 4 GPa, higher than the value reported in the literature (~ 2 GPa). Hence, it is believed that the first signs of plastic deformation occurred at lower loads than the predicted loads from the log scale analysis procedure and is expected to occur as discrete bursts. Discrete plastic events or "pop-ins" were observed in the load-depth indentation responses under quasistatic loading

conditions, which were believed to be associated with shear band activity. An attempt was made to formulate a mathematical model based on three yield criteria (Drucker-Prager, Mohr-Coulomb and von Mises). Based on the von Mises predictions and comparable experiments on a quartz standard, it was established that the pop-ins observed were real and not an instrument artifact. Multiple load cycles following partial unload experiments showed that the pop-ins affected the subsequent indentation response. The moduli and the yield strength values obtained for the Cu-based BMGs were comparable to the values reported in the literature. There was significant scatter in the indentation data from the Fe-based BMG. Porosity and lack of 100 % compaction were believed to be the reasons for scatter in the data.

The financial support of NSF through grant DMR 0314212 is gratefully acknowledged.

ACKNOWLEDGMENTS

With a deep sense of gratitude, I wish to express my sincere thanks to my advisor, Professor Raj Vaidyanathan for his immense help and guidance all along. I would like to express my sincere thanks to Professor C. Suryanarayana for all his help and valuable suggestions during the course of this research. Thanks are due to Professor Helge Heinrich for agreeing to be on my thesis committee.

The cooperation and selfless help that I received from the staff of AMPAC and MMAE, friends and colleagues are greatly acknowledged.

I wish to thank my parents, who taught me the value of sincerity and hard work. I would like to share this moment of happiness with my parents and sister. They extended their unequivocal support during the course of my research. I am grateful to my husband Sudhir for the inspiration and moral support he provided throughout the course of my work. His loving support and readiness to assist helped me complete my present work with ease.

Finally, I would like to thank all whose direct and indirect support helped me complete my thesis in time.

I take this opportunity to acknowledge NSF (DMR 0314212) for funding this research.

TABLE OF CONTENTS

LIST OF FIGURES

LIST OF TABLES

CHAPTER 1 : INTRODUCTION

1.1 Motivation

Instrumented indentation is a novel characterization technique that has rapidly evolved as a powerful tool to assess the mechanical properties of nano- and micro scale volumes and structures [1]. The testing requires only small sampling volumes and consequently can be used to test materials not conveniently available in bulk volumes. This characterization technique can be used over multiple length scales; and it probes the multiaxial deformation characteristics of a material. Such a technique has many advantages and these have been highlighted in chapter 3. Over the past few years instrumented indentation tests at multiple length scales are being used to assess a variety of multi-axial deformation characteristics of bulk metallic glasses in a systematic manner. Bulk Metallic Glasses (BMGs), also known as amorphous metals, have been of considerable scientific and commercial interest because of the unique deformation characteristics owing to their random or chaotic structure, making them attractive for practical applications as a new class of structural as well as functional materials [2]. Instrumented indentation is ideally suited for characterizing these materials because it provides an effective way for studying the deformation behavior of BMGs at nano, micro- and macro- levels via experimental and combinatorial compositions. This is significant because this obviates the need to cast relatively large samples for property extraction via conventional mechanical tests, resulting in substantial reduction in costs.

Thus far researchers have used instrumented indentation to probe various aspects of the deformation behavior of metallic glasses like investigation of the serrated flow during

nanoindentation, the effect of shear band interaction on the serrated flow, a modified yield criterion capturing an important characteristic of metallic glasses through computational approaches etc.

A comprehensive analytical model that predicts the yield strength of a BMG from instrumented indentation was not available in the literature, to the best of the author's knowledge and the use of multi scale instrumented indentation to study the multi axial deformation characteristics of BMGs considering the effect of size scale was lacking. In this regard, a methodology was needed to conduct the indentation experiments in a systematic manner.

This motivated the use of the instrumented nanoindenter, the NANOTEST-600 ® manufactured by Micromaterials of Wrexham, UK, for investigations primarily focused on establishing a methodology for using instrumented indentation at nano- and micro- scales to determine the mechanical response of bulk metallic glasses (BMGs) of varying composition, the implementation in Zr-, Cu- and Fe- based glasses primarily focused on deformation in the elastic regime but including preliminary results related to the onset of inelastic deformation and formulation of a mathematical model that predicts the yield strength of metallic glasses.

1.2 Objective

The primary objectives of this work was to –

- develop and implement a methodology for using instrumented indentation with spherical indenters, since the associated geometry results in simpler stress distributions beneath the indenter when compared to a sharp indenter, at nano- and micro- scales to

determine the mechanical response of Zr-, Cu- and Fe- based bulk metallic glasses (BMGs). Investigations will be primarily focused on deformation in the elastic regime but will include preliminary results related to the onset of inelastic deformation,

- develop analytical formulations to extract the instrument compliance. This is necessary to obtain the true deformation of the specimen by isolating the instrument deformation from the raw data,
- establish a quantitative relation between the macroscopic deformation behavior of the above samples to their corresponding load-depth responses, representative of elastic-plastic deformation to their corresponding load-depth curves from instrumented indentation (Figure 1-1); and
- investigate the evolution of discrete plastic events like serrated flow or “pop-ins” (Figure 1-2) under the indenter.

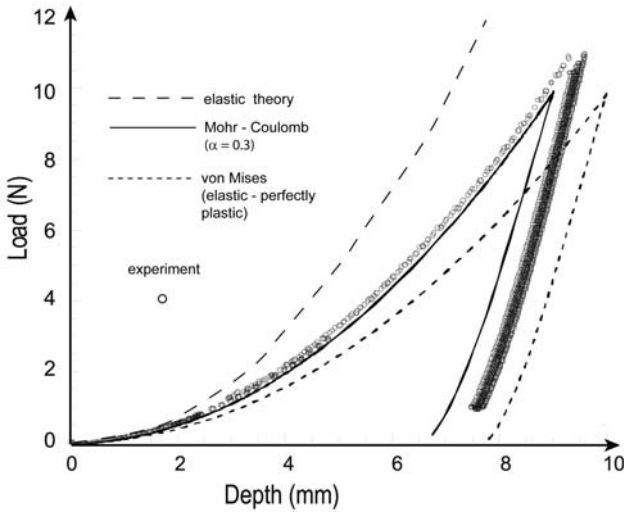

Figure 1-1: A typical load-depth (P-h) response of a Zr-based bulk metallic glass showing that the experimental results are consistent with the Mohr-Coulomb yield criterion, suggesting the influence of a normal component [3] .

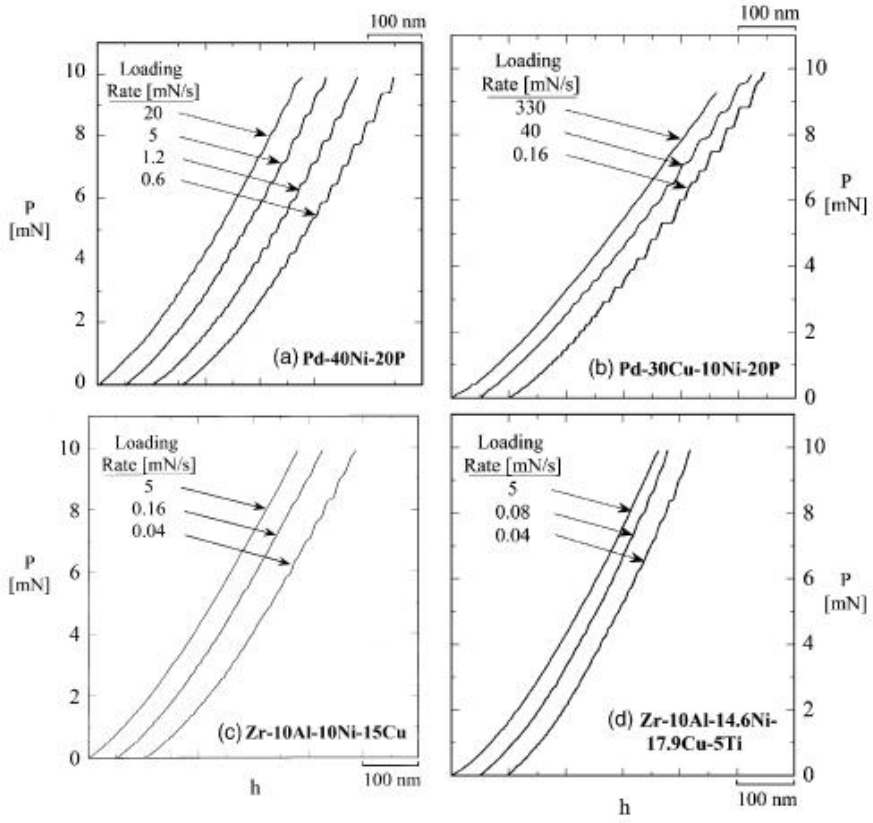

Figure 1-2: Discrete steps or "pop-ins" observed in the load-depth responses of BMG alloys of varying composition with different loading rates specified in each graph [4].

1.3 Organization

This thesis is organized in the following manner:

Chapter Two outlines briefly the history and development of BMGs, summarizes the mechanical behavior and presents some applications of this class of materials.

Chapter Three presents instrumented indentation as a powerful tool for qualitative and quantitative mechanical characterization of nano- and micro scale volumes and structures. A

brief review of the existing methodologies for estimating elastic-plastic properties from representative load-depth data is presented and the principle behind such approaches is emphasized.

Chapter Four describes the work plan which includes various experiments that were performed, the indenters that were used, the experimental parameters and conditions.

Chapter Five presents the standard calibration procedure that was followed prior to indentation of test samples.

Chapter Six presents the results of nanoindentation responses of BMG alloys using different indenters.

Chapter Seven presents the steps in the analysis and discussion of nanoindentation response of BMG samples to extract mechanical properties.

Chapter Eight focuses on conclusions and mentions directions in which this work can be extended.

CHAPTER 2 : LITERATURE REVIEW – BULK METALLIC GLASSES

Bulk metallic glasses or BMGs have generated substantial scientific and commercial interest because of their unique deformation characteristics. This chapter reviews briefly the history of BMGs, their unique properties and the underlying principles and applications of BMGs.

2.1 Introduction

Amorphous metals, also known as metallic glasses, showing random or chaotic structure, as in a liquid, rather than a repeatable, orderly crystalline lattice, have existed in thin ribbon form since the 1960s. Consequently, metallic glasses lack crystalline defects such as grain boundaries and dislocations as in conventional metals. To make bulk glasses, one must frustrate the crystal by atomic mismatch. This mismatch is associated with local atomic-level strains arising from topological differences between the different species in the system. The chaotic structure or the frustration of the crystal structure is typically achieved by rapid cooling the melt from the liquid state. However, high critical quenching rates in the order of 10^5-10^6 K/s imposed a limit on the attainable sizes (typically millimeter scale) for these metallic glasses due to factors like thermal stability and conductivity of these materials during the undercooling process disfavoring the implementation of conventional tensile testing techniques for property estimation and limiting structural applications of the material. With the emergence of BMGs, samples were produced with a critical casting thickness of millimeters to several centimeters.

If one arbitrarily defines the millimeter scale as “bulk”, then the ternary glasses were perhaps the first examples of “bulk” metallic glasses (BMGs) [5]. Detailed reviews on BMGs are available in Ref. [2, 5-9].

2.2 Historical Background and Development of Bulk Metallic Glasses

The first metallic glass was discovered in 1960 by Duwez and co-workers by rapid quenching of a $Au_{80}Si_{20}$ liquid followed by making of amorphous spheres of ternary Pd-Si-M with M = Ag, Cu or Au by Chen and Turnbull [9]. The alloy $Pd_{77.5}Cu_6Si_{16.5}$ could be made glassy with a diameter of 0.5mm and the existence of a glass transition temperature was demonstrated. Earlier Turnbull had predicted that as the ratio of the glass-transition temperature to the melting point of an alloy increased from values near 1/2 to values near 2/3, the homogeneous nucleation of crystals in the undercooled melt should become sluggish on laboratory time scales. This “Turnbull” criterion for the suppression of crystallization in undercooled melts remains today one of the best “rules of thumb” for predicting the glass-forming ability of any liquid [5].

The first detailed studies of crystallization in metallic glasses was done in ternary Pd-Cu-Si and Pd-Ag-Si alloys (due to their large super cooled liquid range of 40 K)[9] . The casting thickness of these alloys were gradually increased by varying the composition and alloying techniques. For instance, Chen made systematic investigations on Pd-T-P alloys (T = Ni, Co, Fe) in 1974 and obtained a critical casting thickness of the order of 1 mm in these alloys. The critical casting thickness of metallic glasses as a function of year the corresponding alloy was developed is shown in Figure 2-1. During the late 1980s, the Inoue group in Sendai,

Japan investigated rare-earth materials with Al and ferrous metals. While studying rapid solidification in these materials, they found exceptional glass-forming ability in La-Al-Ni and La-Al-Cu alloys [10]. Cylindrical samples with diameters of up to 5 mm or sheets with similar thickness were made fully glassy by casting methods.

In the early 1990s, the same group developed Mg-based and Zr-based alloys having a high glass-forming ability. The critical casting thickness in these alloys ranged up to 15 mm. This was followed by development of a quinary alloy $Zr_{41.2}Ti_{13.8}Ni_{12.5}Cu_{10}Be_{22.5}$ by Peker and Johnson, commonly referred to as Vitreloy 1, with a critical casting thickness of several centimeters [11].

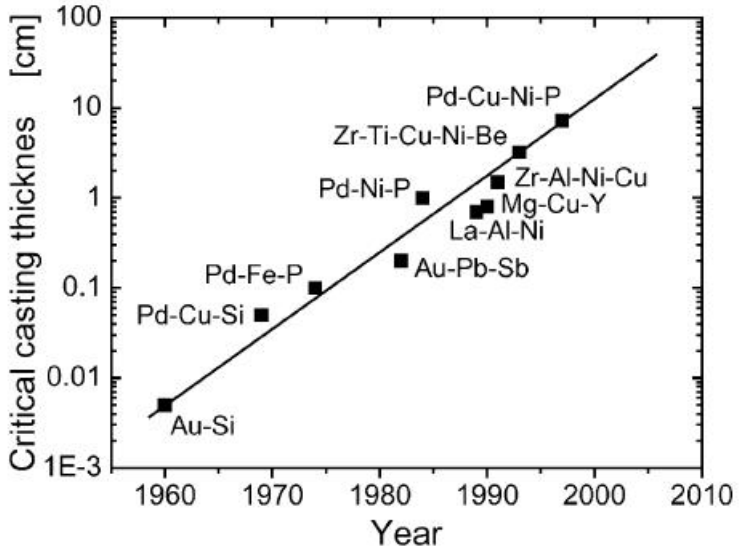

Figure 2-1: The critical casting thickness of metallic glasses as a function of the year developed [9].

2.3 Mechanical Behavior of Bulk Metallic Glasses

Due to the lack of crystalline defects such as grain boundaries and dislocations, unlike conventional metals, BMGs exhibit superior mechanical properties like high strength and hardness, magnetic behavior, and good corrosion resistance. They have large elastic limits (2% - 3%), and high strengths (~ 2 GPa) [12]. BMGs not only exhibit unique mechanical properties but also have a different deformation mechanism in the plastic regime and lack the ability to strain harden in a way seen in conventional metals. For example, in these alloys, plastic deformation is by nucleation and propagation of **shear bands** (Figure 2-2).

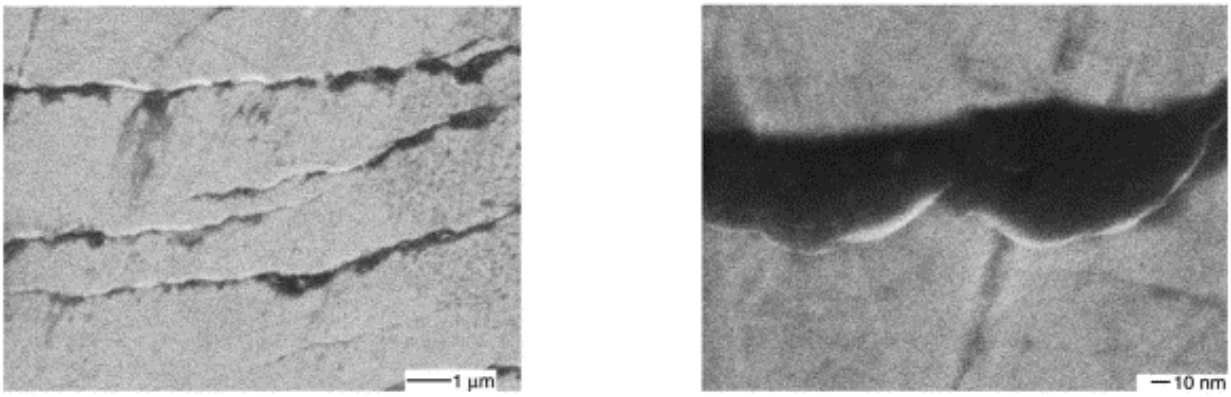

Figure 2-2: Structure of shear bands showing wavy and flowing patterns [3].

Shear bands are extremely inhomogeneous at high stresses and low temperatures and are mechanistically self-organized assemblies of smaller units of plasticity, e.g., volume elements of material containing 30-50 atoms that individually undergo local shear

transformation [13]. Researchers have shown that plasticity in BMGs deviates from the classical von Mises yield criterion, perhaps exhibiting a Mohr-Coulomb yield criterion that is sensitive to both the shear and normal stress components in the plane of shear. Under uniaxial compression at a constant displacement rate, a sample loads elastically until a shear band is initiated at a stress concentration or a region of excess free volume. The load drops as the shear band propagates. The surrounding material elastically recovers, the shear band is arrested, and the process begins again, termed as serrated flow (Figure 1-2).

In amorphous materials, shear bands are expected to form at an angle of 45^{o} to the loading axis under uniaxial compression (plane of maximum shear stress) if there is no normal stress dependence on the slip plane. Experimental evidence found that this angle was 42° and 56° under compression and tension, respectively, indicating that the normal stress which acts across the shear plane influences shear band propagation, associated with the fact that the yielding of metallic glasses follows the Mohr-Coulomb criterion and not von Mises [14-17]. Wright *et al.* showed that this normal stress dependence is expected with the free volume theory [17]. This modified yield criterion captures an important characteristic of metallic glasses, namely that they tend to be stronger in compression than in tension as observed in Figures 2-3 and 2-4.

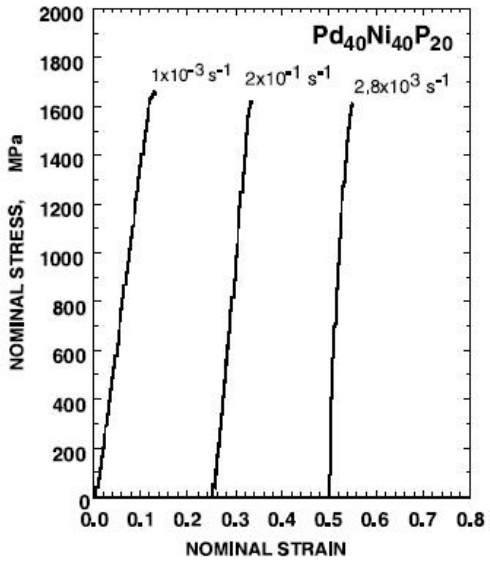

Figure 2-3: The stress-strain response of Pd-based bulk metallic glasses loaded under tension under different loading rates [14].

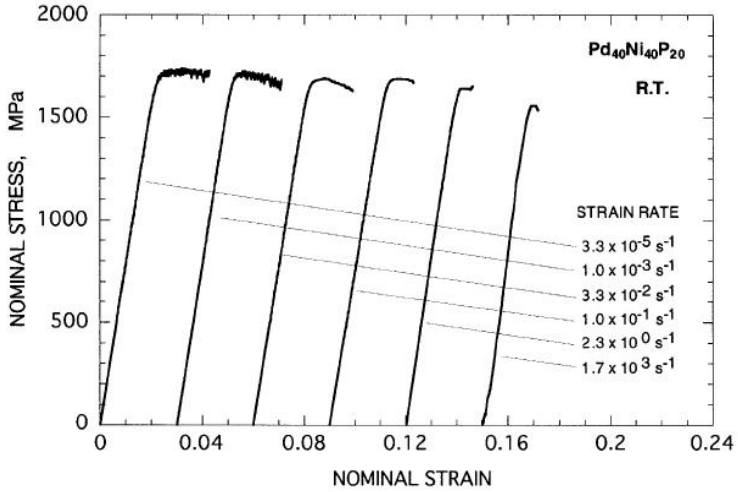

Figure 2-4: The stress-strain response of Pd-based bulk metallic glasses loaded under compression under different loading rates [18].

Researchers have found that under tensile load, there is little global plasticity of the sample as a whole, shear bands are always unconfined and failure is invariably along a single or small number of shear bands and is catastrophic (Figure 2-3). The possibility of enforcing shear-band confinement under tension was demonstrated by Leng and Courtney through fabrication of laminated composite specimens consisting of a layer of metallic glass bonded between two ductile layers [19]. Overall plastic strain of 10 % was achieved.

More recently, the compression tests on a zirconium based alloy by Sergueeva *et al.* illustrated that multiple shear band formation and shear band interaction can lead to strain hardening like behavior in metallic glasses [20], contradicting the belief that shear bands do not interact with one another and the density of shear bands apparently does not change as a function of plastic straining [14]. Quasi-static compression tests by Liu *et al.* on a Zr-based BMG showed multiple shear bands with large plasticity. Microstructural examination demonstrated that slipping, branching and intersecting of multiple shear bands are the main mechanisms for enhancing plasticity as shown in Figure 2-5 [21].

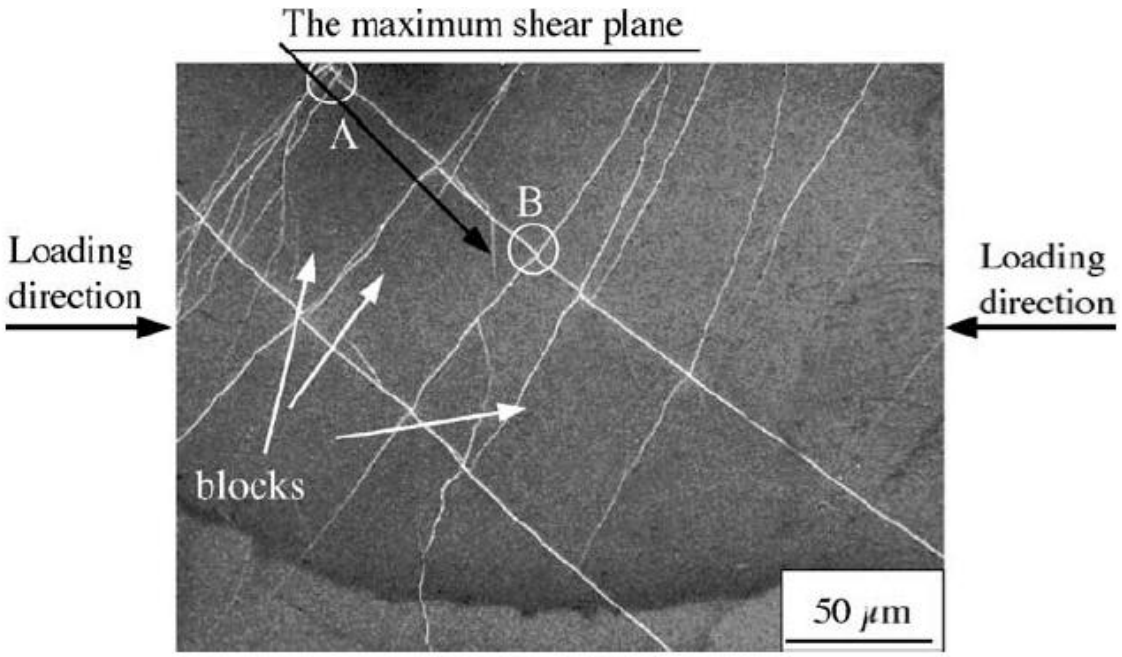

Figure 2-5: Behavior of multiple shear banding observed in a Zr-based bulk metallic glass loaded under quasi-static compression [21].

Thus, it is essential to understand the behavior of shear bands and their role vis-à-vis deformation of metallic glasses to obtain a comprehensive understanding of the deformation behavior of metallic glasses. Substantial research efforts have been invested in studying the shear bands and their role in the deformation of metallic glasses. For example, the model by Edwards *et al.* quantifies shear band propagation in BMGs as a function of the stress tensor, the absolute temperature and the flux of free volume [22]. Hufnagel and Vinci studied the nucleation and growth of shear bands in a zirconium based metallic glass during a three-point bend test using *in situ* scanning electron microscopy [23]. Wright *et al.* reported a reduction in

the viscosity within the shear bands due to a free volume increase which is the primary cause of flow localization with associated heat dissipation [24]. Kanungo *et al.* characterized the distribution of free volume changes associated with deformation of Zr- and Cu- based BMGs using positron annihilation spectroscopy (PAS) [25].

2.4 Applications of Bulk Metallic Glasses

The unique properties of BMGs have generated substantial commercial and scientific interest and have consequently led to their application for varied uses in different fields [7]. BMG is essentially the premier material for the design of springs that can store high densities of elastic energy [5]. This property of metallic glass find its utility in the design of certain types of sporting equipment (e.g., baseball bats [26], golf clubs). Vitreloy 1 has been used in the design of golf club heads. The BMG golf club exploits the high strength, perfectly elastic behavior to accommodate very high strains to improve performance of the golf-club.

Figure 2-6: Applications of bulk metallic glasses – baseball bat featuring “Pure Energy Transfer” [26].

Due to their “self sharpening” ability they find application in armor piercing ammunition casings. Unlike most crystalline metal projectiles, which flatten on impact, the sides of BMGs shear away under dynamic loading. Vitreloy 1 has a highly biocompatible, non-allergenic form, which is ideal for corrosion- and wear-resistant medical applications. For example, DePuy Orthopaedics, Inc. is using the material in knee-replacement devices. Other applications include pacemaker casings [26].

CHAPTER 3 : LITERATURE REVIEW - INSTRUMENTED INDENTATION

This chapter reviews instrumented indentation as a qualitative and quantitative mechanical characterization technique that is applicable to nano- and micro scale volumes and structures. Existing methodologies for estimating elastic-plastic properties from representative load-depth data are briefly reviewed and the principle behind such approaches is emphasized.

3.1 Introduction

Instrumented indentation is a novel characterization technique that has rapidly evolved as a powerful tool that uses small sampling volumes to assess the mechanical properties of materials [1]. In this technique, conducted on a sub-micron regime, the depth of penetration of an indenter, usually a diamond, is measured as a function of the applied load and expressed graphically by what are known as the load (P) – depth (h) curves (Figure 3-1) from which a host of mechanical properties such as Young's modulus, strain-hardening exponent, hardness, etc., can be extracted. Indenters may be sharp (e.g., Berkovich, Vickers, cube corner, etc.), spherical or even flat-ended cylindrical punches. Detailed reviews of instrumented indentation and the associated property extraction techniques can be found in the literature [27].

For the case of bulk metallic glasses, this technique is advantageous because it is ideally suited for small sampling volumes and offers the ability to probe the deformation behavior of the metallic glass under multiaxial loading conditions as the nature of stress under the indenter is multiaxial. Additionally, the spherical geometry results in a simpler stress

distribution under the indenter (when compared to a sharp geometry). More importantly by resorting to spherical indenters the onset of plastic deformation is delayed and can be used over multiple length scales, i.e., nano-, micro- and macro scales, by simply varying the geometry and penetration depth of the indenter. Consequently, multiple test specimens are not needed.

The more prominent advantages of nanoindentation include:

- Sufficiency of small sampling volumes for the technique that obviates the need for fabrication of relatively larger samples for conventional mechanical testing. This is particularly advantageous for experimental and combinatorial compositions,
- It is a technique that can be used over multiple length scales, i.e., nano-, micro- and macro scales, by simply varying the geometry and size of the indenter, and
- It probes the multiaxial deformation characteristics of a material, given that the stress state under an indenter is inherently multiaxial.

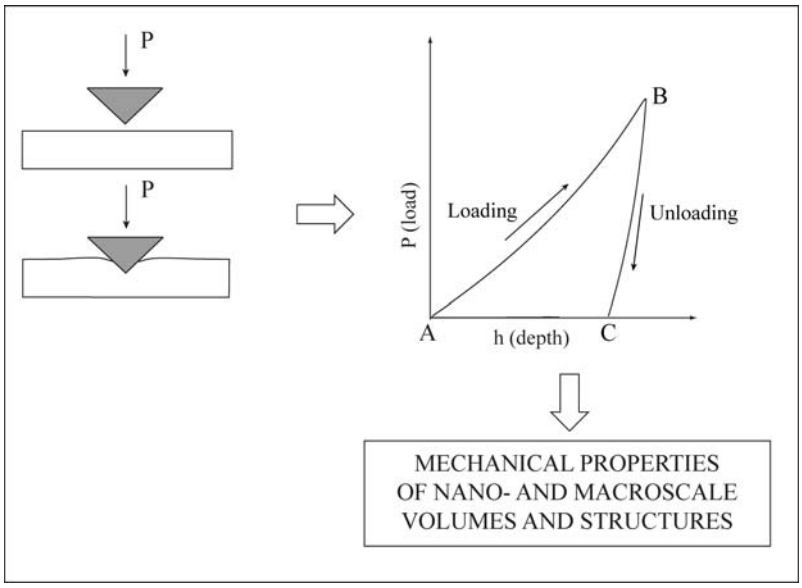

Figure 3-1: The principle of instrumented indentation.

3.2 Property Extraction by Spherical Indentation

A general theoretical framework proposed by Alcala, an extension of the original formulation derived by Hertz that examines the elastic contact between a spherical indenter and a flat surface (infinite radius of curvature) will be used to analyze spherical indentation data [28].

Here the elastic contact is described by

$$P = Ch^{3/2}, \tag{3.1}$$

where the constant C is defined as

$$C = \frac{2\sqrt{2}}{3} E^{*} D^{1/2} . \tag{3.2}$$

In the above equation, D is the indenter diameter and E* the reduced modulus is defined as,

$$E^* = \left(\frac{1-\nu_1^2}{E_1} + \frac{1-\nu_2^2}{E_2} \right)^{-1} . \quad (3.3)$$

The maximum shear stress under the indenter, τ_{max}, as suggested by Johnson [29] will be estimated by using the following expression,

$$\tau_{max} = 0.31 \left(\frac{6PE^{*2}}{\pi^3 R^2} \right)^{1/3} . \quad (3.4)$$

In the above equation, P is the load, R is the indenter radius, E* is a reduced modulus related to the indenter and the specimen, E_1 and ν_1 represent the elastic modulus and the Poisson's ratio of the indenter respectively and E_2 and ν_2 those of the material being indented. The E and ν values for the indenter (diamond) are 1141 GPa and 0.07 respectively.

The elastic modulus of the material subjected to spherical indentation is obtained from the load-depth response of the material, essentially containing the initial elastic portion (in the loading portion of the curve) that follows the aforementioned Hertzian law. A 3/2 power fit to the initial elastic portion of the load-depth curve provides a value for the constant C and the elastic modulus will be derived using the Equations 3.1 - 3.3. Also, any deviation from this slope of 3/2 on a log load vs. log depth plot indicates a deviation from the elastic behavior, which marks the onset of large scale plastic deformation.

During indentation, the machine also deforms along with the material. Hence, the overall depth from the nanoindentation response which is the instrument response coupled with the sample, can be formulated as,

$$h_{total} = h_{instrument} + h_{sample}. \quad (3.5)$$

The instrument compliance is determined by elastically indenting a standard steel specimen of known modulus. As an added check, the machine compliance determined using steel was used to determine the modulus of a fused quartz standard using Equations 3.1 - 3.3 and verified whether values obtained were within error limits of the standard.

3.3 Instrumented Indentation of Bulk Metallic Glasses

There has been a lot of interest in exploring the various aspects of deformation behavior of metallic glasses using instrumented indentation. One of the main uses of instrumented indentation beyond simple measurement of hardness or modulus is to identify discrete events associated with structural changes beneath the indenter [30]. Researchers have found that the deviation from elastic behavior coincides with the first pop-in event. Such an analysis has been carried out by Wright *et al.* to identify the elastic-plastic transition in a Zr-based metallic glass [17]. A detailed review of instrumented indentation studies on BMGs is available in Ref. [30]. Vaidyanathan *et al.* used finite element modeling along with instrumented sharp indentation to show that BMGs follow a pressure sensitive Mohr-Coulomb yield criterion (Figure 1-1) [3]. Patnaik *et al.* conducted finite element simulations of spherical indentation of a Zr-based BMG and compared the results with experimental data and showed that both the hardness and the plastic zone size associated with spherical indentation depend on the yield strength as well as the pressure sensitivity index of the material [31]. Nanoindentation experiments by Greer *et al.* relate the discrete steps in the loading portion of the load-depth curve to shear band initiation

[32]. Schuh *et al.* investigated serrated flow during nanoindentation on several metallic glass materials and noticed that at high loading rates, the load-depth curves were quite smooth while discrete pop-ins were observed only at quasi-static loading conditions [4]. Schuh *et al.* investigated the transition from localized to homogenous plasticity during nanoindentation of a Pd-based BMG under various loading rates [33].

The investigation by Tang *et al.* showed that stepped load-depth curves, corresponding to the serrated flow during nanoindentation experiments, occurred at very low loading rates [34]. Similarly nanoindentation experiments by Liu and Chan on two different Zr-based BMGs exhibited significant serrated plastic flow at low loading rates and also noticed that the serration behavior was pronounced in one of the alloy compositions than the other attributing the difference to the microstructures of the two different Zr-based BMGs [35]. At very high loading rates, serrated flow is fully suppressed. They attributed this to the kinetic limitation for shear band propagation. When the applied loading rate is low, a single shear band can rapidly accommodate the deformation and thus serrated flow occurs. In contrast, when the loading rate exceeds the rate of relaxation by a single shear band, multiple shear bands have to operate simultaneously and lead to smooth load-depth curves.

Anand and Su used a numerical approach to investigate the volume effects and size scale effects on deformation behavior of Zr-based BMGs [36]. More recently Tang *et al.* qualitatively investigated the effect of shear band interaction on the serrated flow behavior of a Zr-based metallic glass using nanoindentation and proposed that the pre-introduced shear bands prevent new shear band formation leading to more serrated flow [34]. Yang *et al.*

observed hardening and recovery phenomena in a Zr-based BMGs using instrumented indentation [37].

CHAPTER 4 : SPECIMENS AND EXPERIMENT OVERVIEW

Instrumented indentation on BMGs of different compositions was carried out to identify and study the various deformation characteristics (highlighted in Chapter 2). This chapter highlights the materials and the indenters used, the work plan, experimental methods and set-up, the various parameters used and precautions observed.

4.1 Work Plan

4.1.1 Material

The materials used in this study were -

- as-cast fully amorphous Zr-based BMG, $Zr_{41.25}Ti_{13.75}Cu_{12.5}Ni_{10}Be_{22.5}$ (nominal composition in at.%) alloy, manufactured by Howmet Corporation, Greenwich, CT (Vitreloy 1) with dimensions of 2 x 0.7 x 0.3 cm
- 30 hours double SPEX® and single SPEX® milled Fe-based BMG samples consolidated by hot isostatic pressing (HIP) and magnetic compaction techniques, $Fe_{60}Co_7Zr_{10}Mo_5W_2B_{16}$ (nominal composition in at.%) samples, and
- as-cast 2.5 mm diameter rods of Cu-based BMGs, $Cu_{60}Hf_{25}Ti_{15}$ and $Cu_{60}Zr_{30}Ti_{10}$ (nominal composition in at.%) alloys.

4.1.2 Indenters

Spherical indentation experiments were carried out on the Nanotest - 600 (Micromaterials Limited, Wrexham, UK). Custom 2.8 mm, 2.0 mm and 100 μm diamond spherical indenters were used. It was ensured that all requirements for hardness measurements were met, such as the measurements were not done close to the edge of the sample and all the depth measurements done were less than one tenth the thickness of the sample.

4.1.3 Conditions

Care was taken to ensure that the machine was not subjected to thermal or vibrational disturbances. Every time the experiment was set up, a time span of at least 30 minutes was allowed for the machine to stabilize thermally, before taking any measurements. The sample surface has to be smooth, not only for consistent results but also for proper operation of the machine. Having said that, measurements can be made on “rough” samples and still obtain accurate results. If a sample is too “rough” then the indenter tip may dash laterally with any protrusion on the surface of the sample, when the sample is moved from one indent location to another indent location. In such cases, the sample retraction distance after each indent can be set to a higher value depending upon the roughness of the sample. For example, if the surface roughness is 100 μm then the sample retraction distance should be set to a value higher than 100 μm. Additionally, porous samples should be avoided as this may not only yield inaccurate results but may also end up harming the pendulum (especially on the fragile NT head) in the long run.

It was ensured that the surface on the specimen to be indented and the corresponding back surface were parallel to each other. The sample was glued to a sample holding aluminum stub. The adhesive used for this purpose is extremely fluid and only a thin layer was used to prevent it from introducing any additional compliance. It is important that the machine is well calibrated before performing the indentation on test samples for achieving reliable results. The calibration procedures and the methodology for extraction of machine compliance for Micro and Nano test platforms are described in Chapter 5.

4.1.4 Experiments and Experimental Parameters – Zr-based BMG

For the case of the Zr-based BMG (Vitreloy 1), four different sets of experiments were conducted. In the first, experiment set 1 (A1), the 2.8 mm diameter diamond indenter was used to indent the material to maximum loads of 1 N, 2 N and 4 N at different locations at a loading rate of 100 mN/s. In the second, experiment set 2 (A2), the 100 μm diameter diamond indenter was used to indent the material to a maximum load of 1.5 N at different locations at a loading rate of 100 mN/sec. In the third, experiment set 3 (A3), the 100 μm diameter diamond indenter was used to indent the material to a maximum load of 400 mN at different locations at a loading rate of 1 mN/sec. In the fourth, experiment set 4 (A4), the 100 μm diameter diamond indenter was used to perform multiple load cycle experiments with increasing loads with partial unloading (10%) at the same location at a loading rate of 1 mN/sec. The partial unloading cycle starts at the minimum depth specified and complete unloading occurs at the maximum depth specified. The number of indentation cycles were specified in the module and

were so chosen that the partial unloading was done at a load just after a pop-in event had occurred.

The purpose of experiment set A1 was to probe the elastic behavior. The purpose of experiment set A1 and A2 was to study the effect of indenter size on elastic behavior and the purpose of experiment set A2 was to study the large scale plastic deformation in Vitreloy 1. The purpose of experiment set A3 was to capture discrete plastic events or "pop-ins" and correlate them with the analytical model. In experiment sets A2, A3 and A4 described above, indentations are expected to generate shear bands upon onset of plasticity. Experiment set A3 helps to study the initial plastic events which otherwise were suppressed by large scale plastic deformation. More importantly by resorting to spherical indenters the onset of plastic deformation is delayed and this will provide a means to study such initial plastic events. The purpose of experiment set A4 was to study the change in the load-depth responses following a pop-in event.

4.1.5 Experiments and Experimental Parameters – Cu - based BMG

For the case of the Cu-based BMG, two different sets of experiments were conducted. A custom 100 μm diameter diamond spherical indenter was used. Porosity was observed in the sample during sample preparation. It is believed that the subsequent contact problems that were encountered during the indentation of this specimen using a 2.0 mm and a 2.8 mm diameter diamond spherical indenter, were because of the large volume of pores.

Indentations were done along the radial direction of the sample using the 100 μm diameter diamond spherical indenter. In the first, experiment set 1 (B1), the 100 μm diameter

diamond spherical indenter was used to indent $Cu_{60}Hf_{25}Ti_{15}$ at various locations to a maximum load of 1 N. In the second, experiment set 2 (B2), the 100 μm diameter diamond indenter was used to indent $Cu_{60}Zr_{30}Ti_{10}$ at various locations to a maximum load of 1 N. The purpose of experiment sets B1 and B2 was to probe the elastic-inelastic behavior of the Cu-based BMG samples.

4.1.6 Experiments and Experimental Parameters – Fe - based BMG

For the case of the Fe-based BMG, two different sets of experiments were conducted. The custom 2.8 mm diameter diamond spherical indenter was used. In the first, experiment set 1 (C1), the 2.8 μm diameter diamond spherical indenter was used to indent the 30 hours double SPEX milled and HIPed $Fe_{60}Co_7Zr_{10}Mo_5W_2B_{16}$ sample at different locations to a maximum load of 750 mN. In the second, experiment set 2 (C2), the 2.8 mm diameter diamond spherical indenter was used to indent the 30 hours single SPEX milled and HIPed $Fe_{60}Co_7Zr_{10}Mo_5W_2B_{16}$ sample at different locations to a maximum load of 750 mN. The purpose of experiment sets C1 and C2 was to probe the elastic behavior of the Fe-based BMG sample.

CHAPTER 5 : CALIBRATION PROCEDURE

5.1 High Load Indentation – Micro Test Platform

5.1.1 Calibration of the Instrument

As mentioned earlier in Chapter 3, during indentation, the machine also deforms along with the material. Figure 5-1 shows the raw load-depth response obtained by elastically indenting a standard steel specimen and the expected load-depth response of the steel. Figure 5-2 shows the instrument response determined by subtracting the expected response of steel from the corresponding raw load-depth response. The instrument compliance or the machine's deformation was determined by subtracting the expected response of steel from the corresponding raw load-depth response got by elastically indenting a standard steel specimen of known modulus. The load-depth response of the instrument was linear in the case of the Micro Test platform as seen in Figure 5-2.

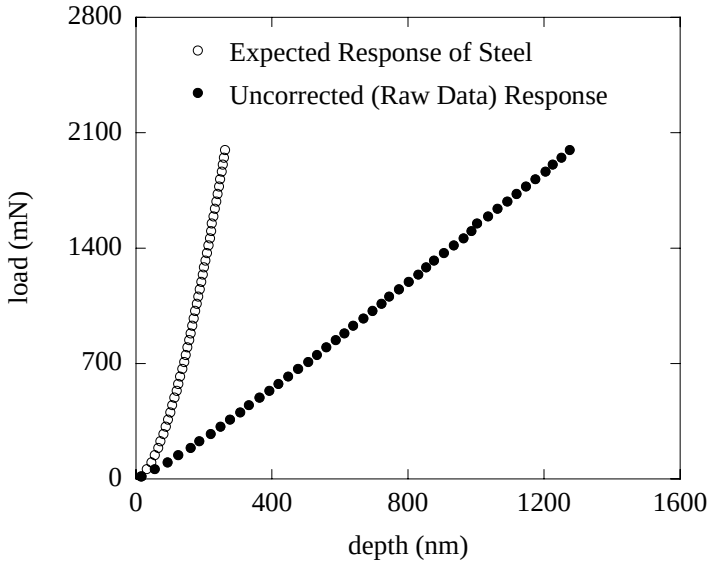

Figure 5-1: Expected and uncorrected (raw) load-depth response of steel obtained by indenting with a 2.8 mm diameter diamond spherical indenter for instrument compliance calibration on the Micro Test platform.

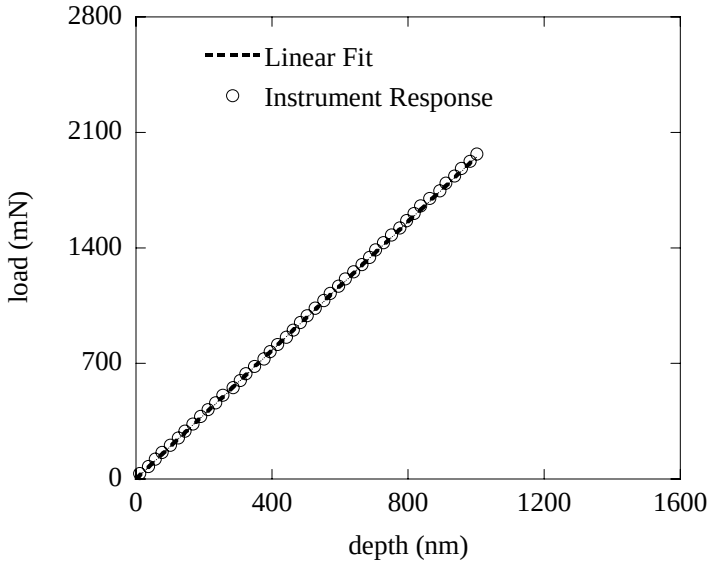

Figure 5-2: Load-depth response of the instrument on the Micro Test platform. Load-depth response of the instrument obtained by elastically indenting a standard steel specimen of known modulus using a 2.8 mm indenter.

5.1.2 Verification of the Instrument Compliance using a Standard

As an added check, for verification of instrument compliance, the material's load-depth response is determined by elastically indenting a standard quartz specimen (of known modulus) and verified whether the values obtained for the modulus are within error limits of the standard. The elastic modulus of quartz subjected to spherical indentation was obtained from the corresponding load-depth response, essentially containing the initial elastic portion (in the loading portion of the curve) that followed the afore mentioned Hertzian law. A 3/2 power fit to the initial portion of the load-depth curve provided a value for the constant C and the elastic modulus was derived using Equations 3.1 - 3.3. The elastic modulus of fused quartz sample was found to be 71.8 $\pm$ 0.7 GPa, which is in good agreement with the modulus of quartz (72 GPa).

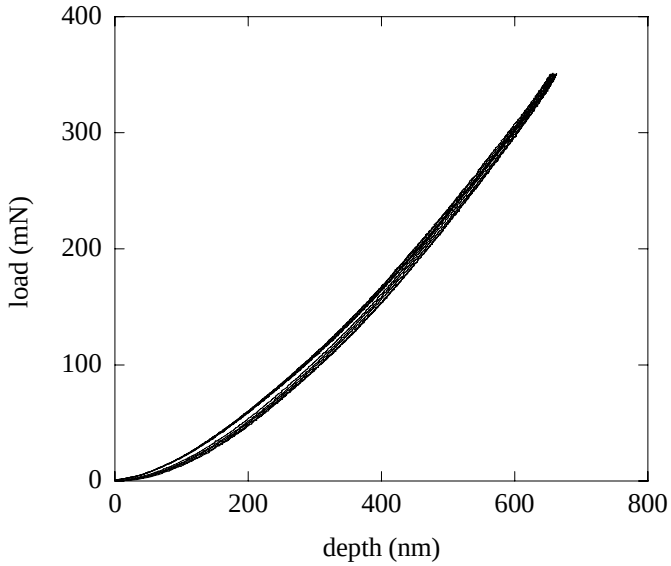

Figure 5-3: Verification of instrument compliance using a standard (fused quartz). Load-depth response of quartz obtained by indenting using a 2.8 mm indenter.

5.2 Low Load Indentation – Nano Test Platform

As mentioned earlier in section 5.1, the instrument compliance or the machine deformation was determined by subtracting the expected response of steel from the corresponding raw load-depth response got by elastically indenting a standard steel specimen of known modulus. The load-depth response of the machine deformation followed a 3/2 slope in the case of the Nano Test platform (Figure 5-4) when indented using a 100 μm indenter, a behavior different from that of the Micro Test platform.

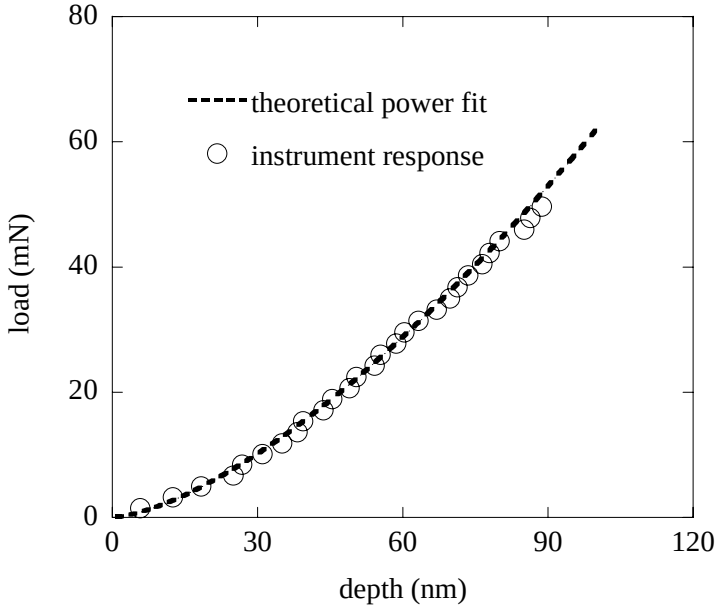

Figure 5-4: Instrument compliance calibration for the Nano Test platform. Load-depth response of the instrument obtained by elastically indenting a standard steel specimen of known modulus using a 100 μm indenter.

When the machine's deformation displays considerable elastic recovery that follows a 3/2 power law, there is no existing model to determine the machine deformation. This results in considerable difficulty in obtaining valid mechanical property data for characterizing the materials using instrumented indentation at nano scales. An alternative approach, described here, is to attempt to understand the spherical indentation loading curves and thus quantitatively model the relationship between machine and material deformation, so that this methodology could be applied for low load indentations on the Nano Test platform and subsequently extended to Vitreloy 1 and other materials of interest.

5.2.1 Formulation of Double Contact Problem

Based on the load-depth response (Figure 5-4) of the machine, the indenter-material surface has been modeled as shown in Figure 5-5.

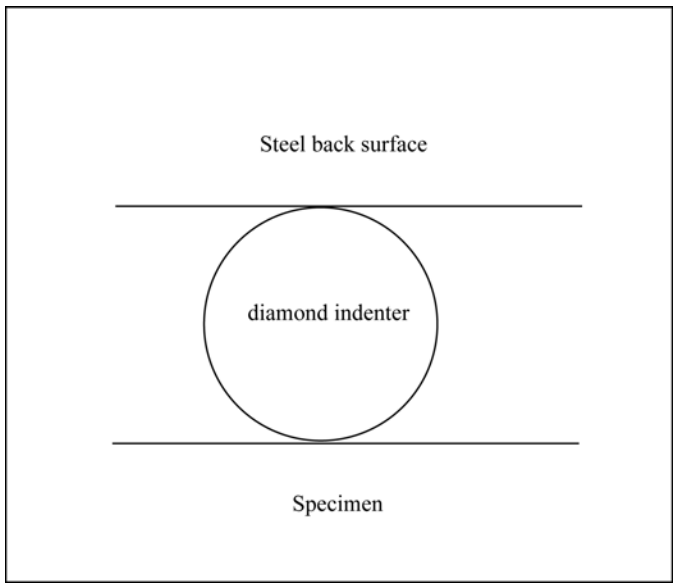

Figure 5-5: Proposed indenter-material surface model for the Nano Test platform.

The overall depth from nanoindentation which is the instrument response (back surface and the indenter) coupled with the specimen response under elastic conditions, can be formulated as

$$h = h_{\text{back surface and indenter}} + h_{\text{sample}}. \quad (5.1)$$

As per the Hertzian formulation that examines elastic contact between a spherical indenter and a flat surface (infinite radius of curvature), the elastic contact is described by

$P = Ch^{3/2}$ (for elastic deformation).

The parameter C needs to be determined. Based on the observed load-depth response of the instrument (Figure 5-4), the proposed model and the parameters needed for analysis of the data, the parameter C was partitioned and defined as follows.

C_b - contact compliance between steel back surface and indenter.

C_s - contact compliance between indenter and specimen.

C - total compliance corresponding to total measured depth h (from the raw data) for elastic conditions.

The objective was to relate C, C_b and C_s.

As shown in Figure 5-4, the instrument (back surface coupled with indenter) and the material followed a 3/2 power law under elastic conditions. The depths $h_{\text{back surface and indenter}}$ and h_{sample} were defined based on the Hertzian formulation as follows:

$$h_{\text{back surface and indenter}} = \left(\frac{P}{C_b}\right)^{\frac{2}{3}} \text{ and}$$

$$h_{\text{sample}} = \left(\frac{P}{C_s}\right)^{\frac{2}{3}}.$$

Further by substituting for $h_{\text{back surface and indenter}}$ and h_{sample} in Equation (5.1), the overall depth h was expressed as

$$h = \left(\frac{P}{C_b}\right)^{\frac{2}{3}} + \left(\frac{P}{C_s}\right)^{\frac{2}{3}}. \qquad (5.2)$$

Rearranging Equation (5.2) in terms of load P gives

$$P = C_s \left[\left(\frac{C_s}{C_b} \right)^{\frac{2}{3}} + 1 \right]^{\frac{-3}{2}} h^{\frac{3}{2}}. \tag{5.3}$$

Correlating Equation (5.3) with the Hertzian formulation, for elastic deformation gives

$$C = C_s \left[\left(\frac{C_s}{C_b} \right)^{\frac{2}{3}} + 1 \right]^{\frac{-3}{2}} \tag{5.4}$$

where, the parameter C, the total compliance was determined by fitting a 3/2 curve to the initial elastic portion of the loading curve of the raw load-depth response obtained by indenting steel of known modulus.

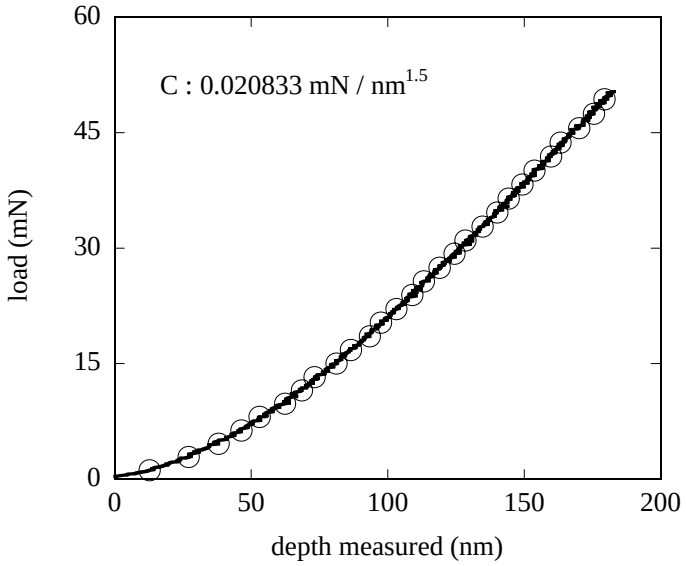

Figure 5-6: Overall load-depth response of steel indented using a 100 μm indenter to extract the machine compliance.

As per the proposed indenter-material surface model for the Nano Test platform, the back surface is made of steel. By indenting a standard steel specimen elastically, C_b was related to C_s through Equation (5.5) as

$$C_b = C_s. \tag{5.5}$$

By Equation (5.5), the parameter C_s is related to C by replacing C_b in terms of C_s in Equation (5.4) as

$$C = C_s \left(2\right)^{\frac{-3}{2}}. \tag{5.6}$$

As mentioned earlier, the value of C was obtained by indenting steel using a 100 μm indenter of known modulus.

From experiments (Figure 5-6), $C = 0.020833\ mN/nm^{1.5}$.

Using the value of C in Equation(5.6), gives $C_s = 0.059\ mN/nm^{1.5}$. (5.7)

From Equation (5.5), $C_b = C_s = 0.059\ mN/nm^{1.5}$.

The elastic modulus of the steel specimen corresponding to C_s using Equations (3.1) – (3.3) was found to be 213 GPa, very close to the actual modulus of steel (210 GPa).

The next step was to verify this formulation.

5.2.2 Verification of the formulation using another Specimen – Vitreloy 1

For verification purposes, the parameters C_b, C_s and C defined earlier had to be determined and verified on Vitreloy 1.

From Equation (5.4),

$$C = C_s \left[\left(\frac{C_s}{C_b} \right)^{\frac{2}{3}} + 1 \right]^{\frac{-3}{2}}.$$

As per Equation (5.7), $C_b = 0.059\ mN/nm^{1.5}$.

For an expected load-depth response of Vitreloy 1, $C_s = 0.0312\ mN/nm^{1.5}$.

Substituting for C_b and C_s in Equation (5.4), gives $C = 0.0147\ mN/nm^{1.5}$.

Substituting for C in the Hertzian formulation gives $P = 0.0147\ h^{1.5}$, which is the predicted response of Vitreloy 1 for total depth h, as C corresponds to total depth h.

Figure 5-7 shows the predicted load-depth response for total depth h and the experimental raw data obtained by indenting Vitreloy 1.

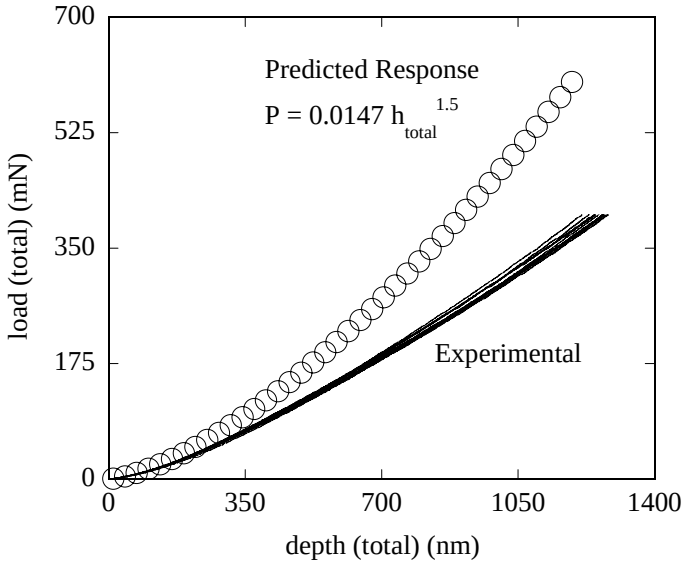

Figure 5-7: Raw data (load-depth response) obtained by indenting Vitreloy 1 using a 100 μm indenter compared with the predicted load-depth response.

The difference in depth between the predicted and the experimental response resulted in a linear relation as shown in Figure 5-8. This was believed to be an influence of another linear variable affecting the contact between the back surface and the indenter. Hence the model was reformulated by introduction of a linear machine compliance relation accounting for this linear response.

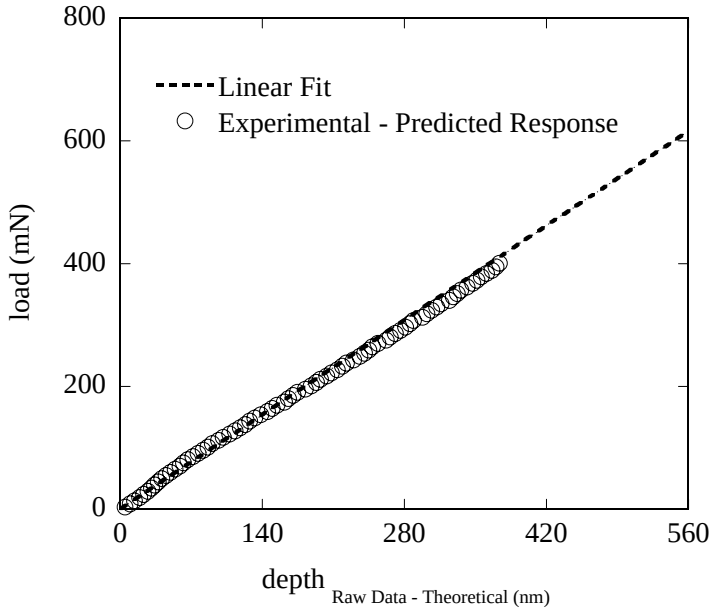

Figure 5-8: Load-depth graph obtained by plotting the load and the difference in depth between the predicted response and the experimental response.

5.2.3 Reformulation of the Double Contact Problem

Reformulation of the double contact problem was based on the introduction of a new linear response (machine compliance relation) to the overall load-depth response.

The contact compliances were defined as follows for reformulating the model:

C_b - Contact compliance between the steel back surface and the indenter

C_s - Contact compliance between the indenter and the specimen

C_m - Compliance of machine

C - Total compliance corresponding to total measured depth h (from the raw data) for elastic conditions.

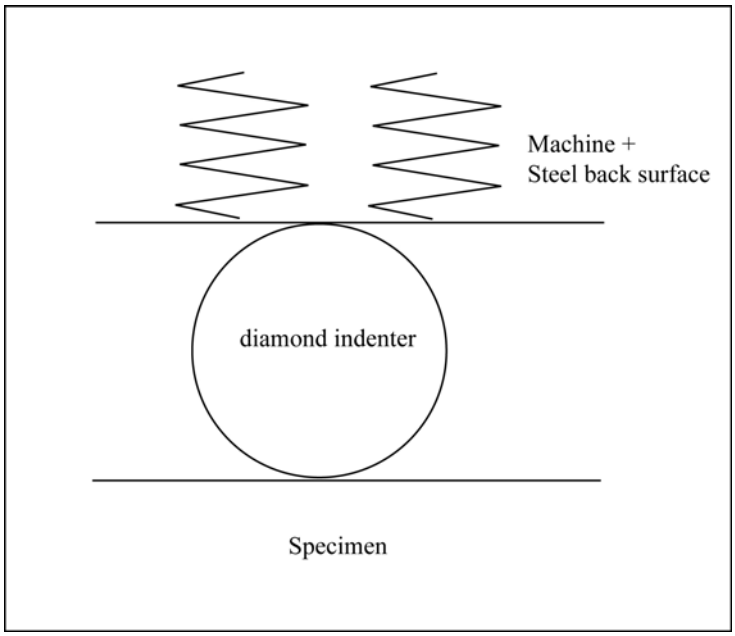

Figure 5-9: Improved indenter-material surface model for the Nano Test platform.

The total indentation depth was rewritten as

$$h_{measured} = h_{sample} + h_{back\,surface} + h_{machine}. \tag{5.8}$$

The terms in Equation (5.8) were defined as

$$h_{sample} = \left(\frac{P}{C_s}\right)^{\frac{2}{3}}$$

$$h_{back\,surface} = \left(\frac{P}{C_b}\right)^{\frac{2}{3}}$$

$$h_{machine} = \left(\frac{P}{C_m}\right).$$

Further by rearranging Equation (5.8), an expression for $h_{back\ surface}$ and $h_{machine}$ was obtained as

$$h_{back\,surface} + h_{machine} = h_{measured} - h_{sample}.$$

Substituting for $h_{back\ surface}$ and $h_{machine}$ in terms of load P and their respective compliances yielded the relation

$$h_{backsurface} + h_{machine} = \left(\frac{P}{C_b}\right)^{\frac{2}{3}} + \left(\frac{P}{C_m}\right). \tag{5.9}$$

Equation (5.9) was generalized as,

$$h_{back\,surface} + h_{machine} = G_0 P^{\frac{2}{3}} + G_1 P, \text{where } G_0 = \frac{1}{C_b^{\frac{2}{3}}} \text{ and } G_1 = \frac{1}{C_m}. \tag{5.10}$$

The parameters C_b and C_m were obtained using a semi analytical code (using MathCAD). A function H(P,G) was defined to find the constants G_0 and G_1. A guess function was used to estimate the values of G_0 and G_1 through appropriate curve fitting of the function H(P,G). Consequently, the value of compliances of the machine and the back surface C_b and C_m were obtained using Equation (5.10).

The function H(P,G) was defined as follows

$$H(P,G) = \begin{bmatrix} G_0 P^{\frac{2}{3}} + G_1 P \\ P^{\frac{2}{3}} \\ P \end{bmatrix}.$$

A guess function was defined to find the constants G_0 and G_1 as $guess := \begin{pmatrix} 2 \\ 2 \end{pmatrix}$, so that $G := genfit\left(load, h_{machine+back\ surface}, guess, H\right)$.

This semi analytical code gave the values of C_b and C_m. C the total compliance corresponding to total measured depth h (from the raw data) for elastic conditions was obtained by indenting steel of known modulus. Knowing the values of C_b, C_m and C; C_s, the compliance of the sample was calculated. Knowing C_s, the true response of the specimen was obtained.

When a material was indented, irrespective of the choice of material, the machine deformation had to be unique. The next step was to check for the uniqueness of the instrument (machine and back surface) deformation.

5.2.4 Uniqueness of Instrument Deformation

To check for the uniqueness of the instrument, the material standards, steel and quartz were indented using the 2.0 mm diameter diamond spherical indenter. The overall depth from the nanoindentation response based on section 5.2.3, was formulated as

$$h_{total} = h_{back\ surface} + h_{machine} + h_{sample}. \quad (5.11)$$

The parameters were defined based on the section 5.2.3. The parameter C, the total compliance corresponding to total depth h_{total} was determined from the raw indentation data (load-depth response) obtained by indenting steel and quartz of known modulus. As mentioned earlier a 3/2 power fit to the initial elastic portion of the loading curve provided a value for the constant C. Since steel and quartz were standard materials, C_s the contact compliance between

the indenter and the specimen was known. Knowing C and C_s, the expressions for h_{total} and h_{sample} were related to the load P through the Hertzian formulation to give

$$h_{sample} = \left(\frac{P}{C_s}\right)^{\frac{2}{3}}$$

$$h_{total} = \left(\frac{P}{C}\right)^{\frac{2}{3}}$$

For this case, Equation (5.11) maybe written as,

$h_{back\ surface} + h_{machine} = h_{total} - h_{sample}$.

Using the expressions for h_{total} and h_{sample} in Equation (5.11),

$$h_{backsurface} + h_{machine} = \left(\frac{P}{C}\right)^{\frac{2}{3}} - \left(\frac{P}{C_s}\right)^{\frac{2}{3}}. \qquad (5.12)$$

The resulting load-depth response corresponding to machine and back surface deformation were obtained from indentation using Equation (5.12). There was discrepancy in the instrument response obtained from indenting quartz. It was believed to be attributed to the presence of residual stresses in the quartz sample. Another standard material Tungsten was used not only to check for the uniqueness of the instrument response but also to select a suitable material standard for determination of the instrument response.

Tungsten was indented elastically using a 2.0 mm indenter. By applying the formulation mentioned in the section 5.2.3 to the initial elastic portion of the loading curve, the instrument response was obtained. The resulting instrument responses (machine coupled with back surface) obtained from indenting steel and tungsten were compared to check for the uniqueness of instrument deformation as shown in Figure 5-10.

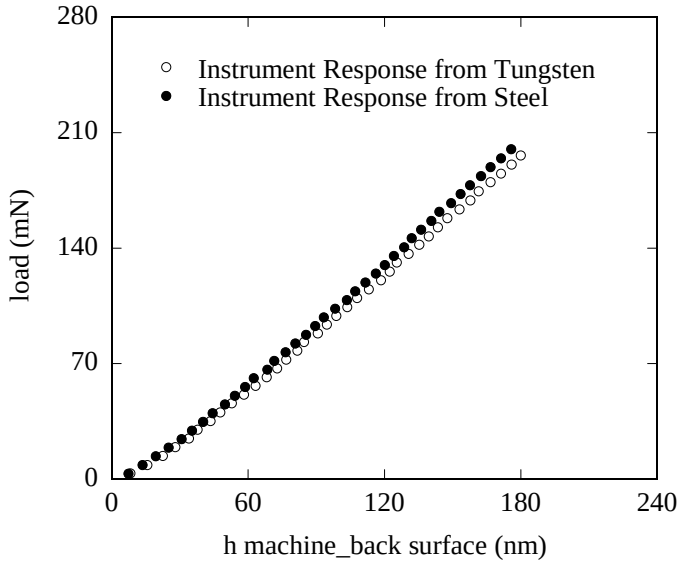

Figure 5-10: The comparison of instrument responses obtained from indenting steel and tungsten samples using a 2.0 mm indenter to check for its uniqueness.

The results showed that the instrument responses obtained from indenting steel and tungsten were quite comparable (Figure 5-10). Consequently it was recognized that steel was an appropriate standard for determination of the overall instrument response following the methodology mentioned in section 5.2.3 and the uniqueness of the instrument response was established. Knowing the instrument response, the true response of the test sample could be obtained.

CHAPTER 6 :RESULTS

Several indentation experiments were conducted on BMG samples of varying composition as detailed in the preceding chapter. This chapter presents the results of those experiments.

6.1 Zr-based Bulk Metallic Glass

Figure 6-1 shows the load-depth response of Vitreloy 1 corresponding to experiment set A1 displaying considerable elastic recovery. Figure 6-2 shows a representative load-depth response of Vitreloy 1 corresponding to experiment set A2.

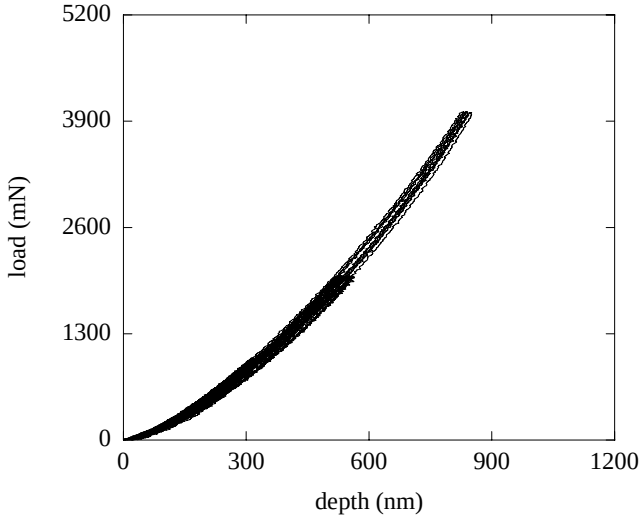

Figure 6-1: Nanoindentation response of Vitreloy 1 indented using a 2.8 mm diameter diamond spherical indenter indented to maximum loads of 1 N, 2 N and 4 N (corresponding to experiment set A1) .

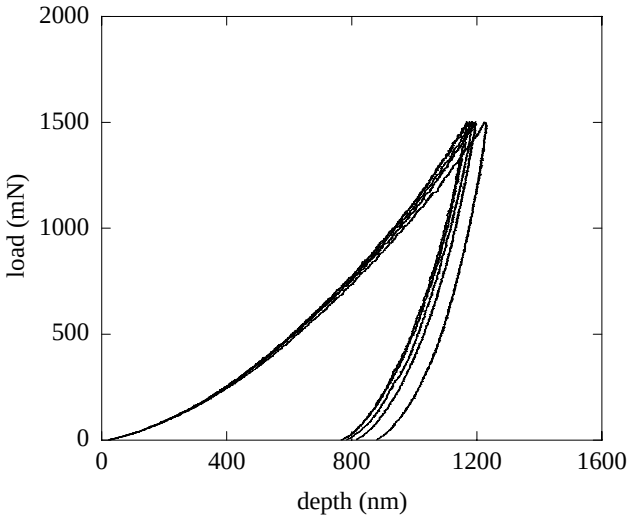

Figure 6-2: Nanoindentation response of Vitreloy 1 indented using a 100 μm diameter diamond spherical indenter indented to a maximum load of 1.5 N (corresponding to experiment set A2).

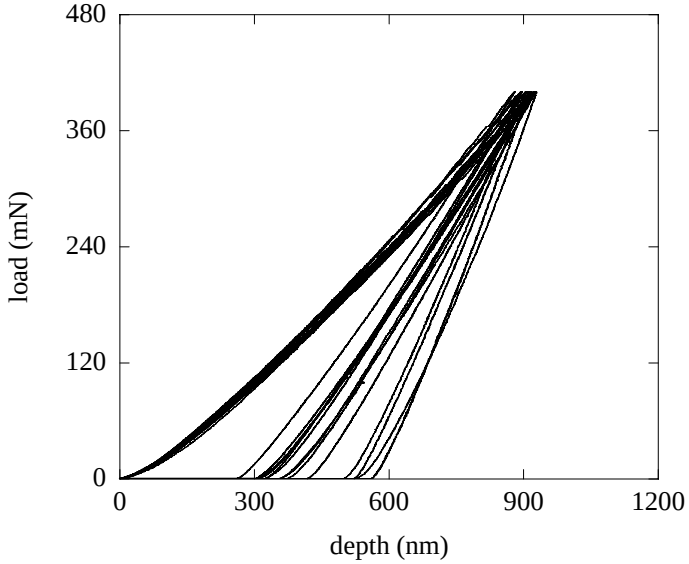

Figure 6-3: Load-depth response of Vitreloy 1 indented using a 100 μm diameter diamond spherical indenter indented to a maximum load of 400 mN (corresponding to experiment set A3).

Discrete bursts or “pop-ins” (Figure 6-4) were observed when Vitreloy 1 was indented quasi statically using a 100 μm diamond spherical indenter (experiment set A3).

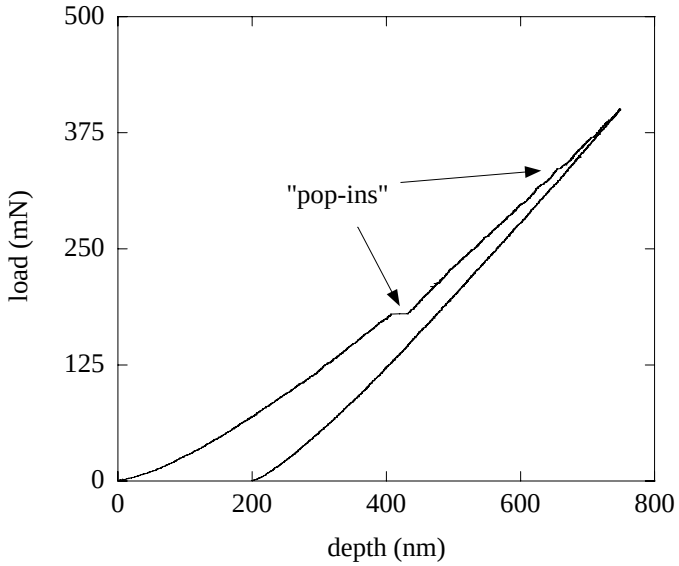

Figure 6-4: Load-depth response of Vitreloy 1 indented using a 100 μm diameter diamond spherical indenter, where the pop-in is likely to be associated with shear band activity (corresponding to experiment set A3).

Figure 6-5 shows the load-depth response of Vitreloy 1 indented with a 100 μm indenter corresponding to experiment set A4. Multiple load cycles with increasing loads were conducted, where the minimum depth specified for the first partial unloading was 160 mN and the maximum depth for complete unloading was specified as 240 mN. The number of cycles was specified as 8.

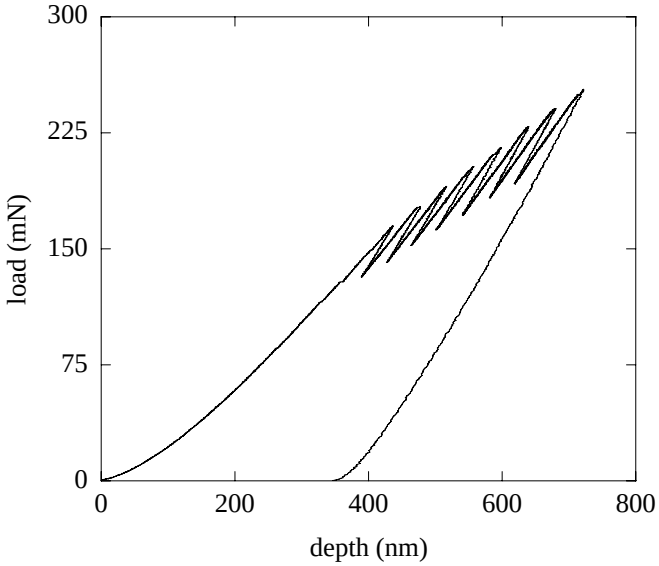

Figure 6-5: Nanoindentation response of Vitreloy 1 indented using a 100 μm indenter in a multiple load cycle (8 cycles) experiment with increasing load and partial unload (corresponding to experiment set A4).

Figure 6-6 shows the load-depth response of Vitreloy 1 indented with a 100 μm indenter corresponding to experiment set A4. In this module, the minimum depth for the first partial unloading was specified as 45 mN and the maximum depth for complete unloading was specified as 290 mN. The number of cycles was specified as 21 in this module to have more number of partial unloading cycles close to the pop-in event.

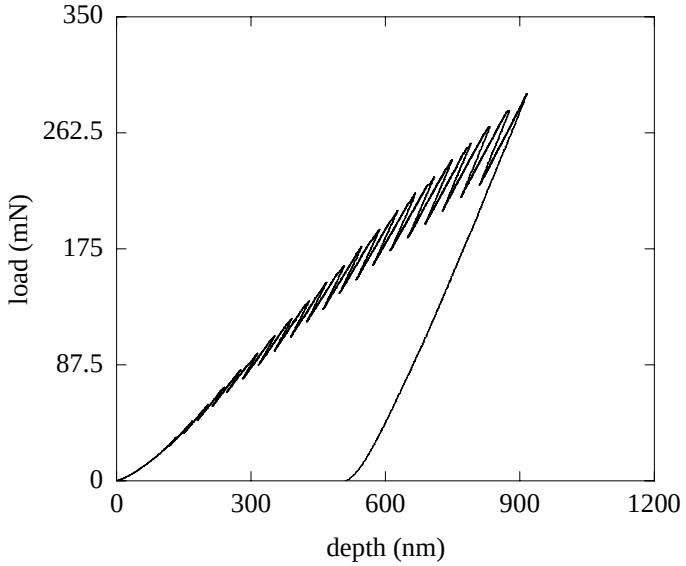

Figure 6-6: Nanoindentation response of Vitreloy 1 indented using a 100 μm indenter in a multiple load cycle (21 cycles) experiment with increasing load and partial unload (corresponding to experiment set A4).

6.2 Cu-based Bulk Metallic Glass

Figure 6-7 shows the elastic-inelastic response of $Cu_{60}Hf_{25}Ti_{15}$ corresponding to experiment set B1. The elastic modulus was found to be 94 $\pm$ 2 GPa using the Hertzian analysis described earlier. Figure 6-8 shows the elastic-inelastic response of $Cu_{60}Zr_{30}Ti_{10}$ corresponding to experiment set B2. The elastic modulus was found to be 98 $\pm$ 5 GPa using the Hertzian analysis described earlier.

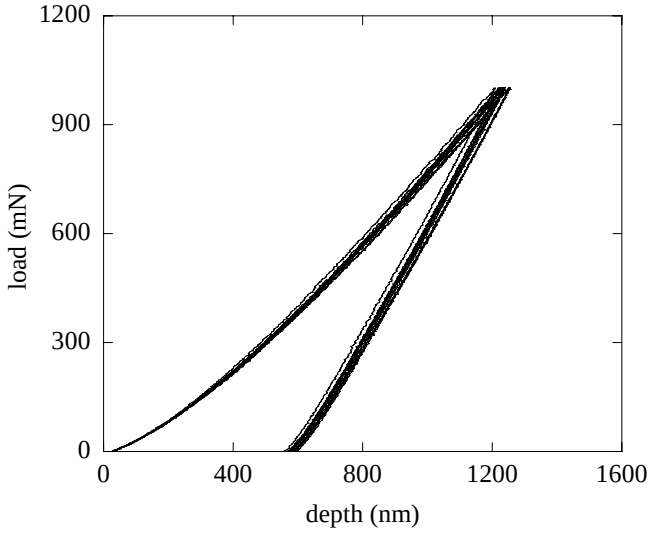

Figure 6-7: Nanoindentation response of $Cu_{60}Hf_{25}Ti_{15}$ alloy indented using a 100 μm diameter diamond spherical indenter (corresponding to experiment set B1).

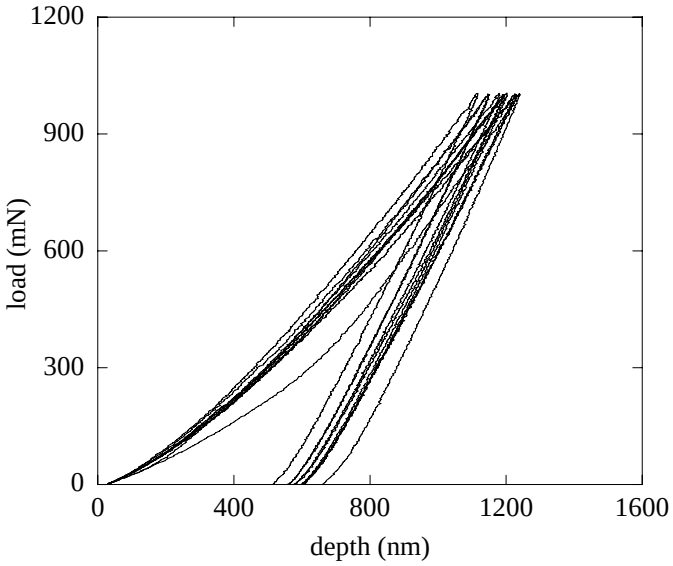

Figure 6-8: Nanoindentation response of $Cu_{60}Zr_{30}Ti_{10}$ alloy indented using a 100 μm diameter diamond spherical indenter (corresponding to experiment set B2).

6.3 Fe-based Bulk Metallic Glass

Figure 6-9 shows the elastic response of $Fe_{60}Co_7Zr_{10}Mo_5W_2B_{16}$ corresponding to experiment set C1. The elastic modulus was found to be 53 $\pm$ 15 GPa using the Hertzian analysis.

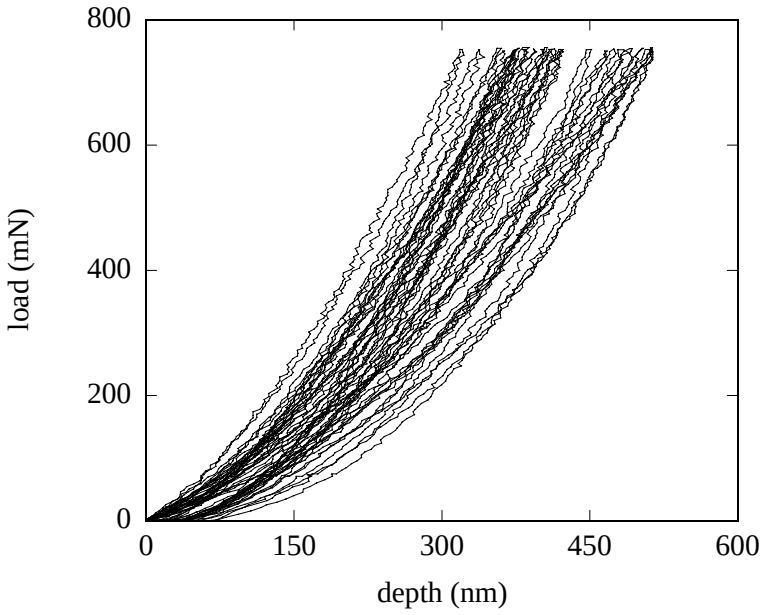

Figure 6-9: Nanoindentation response of the 30 hours double SPEX® milled and consolidated $Fe_{60}Co_7Zr_{10}Mo_5W_2B_{16}$ alloy indented using a 2.8 mm diameter diamond spherical indenter (corresponding to experiment set C1).

Figure 6-10 shows the elastic response of $Fe_{60}Co_7Zr_{10}Mo_5W_2B_{16}$ corresponding to experiment set C2. The elastic modulus was found to be 44 $\pm$ 9 GPa using the Hertzian analysis.

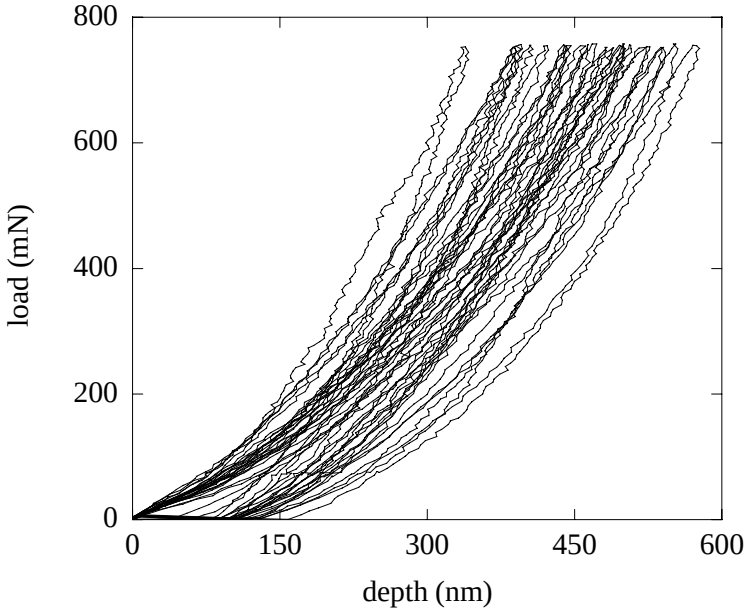

Figure 6-10: Nanoindentation response of the 30 hours single SPEX® milled and consolidated $Fe_{60}Co_7Zr_{10}Mo_5W_2B_{16}$ alloy indented using a 2.8 mm diameter diamond spherical indenter (corresponding to experiment set C2).

CHAPTER 7 : ANALYSIS AND DISCUSSION

This chapter presents the formulation of an analytical model that predicts the yield strength of a metallic glass, an attempt to correlate the model with the experimental data, the analysis of experimental data and the conclusions drawn thereof. Subsequently the results and their implications are discussed.

7.1 Formulation of Mathematical Models

7.1.1 Model Based on Drucker-Prager Yield Criterion

As per the Drucker-Prager Yield Criterion, the functional form can be approximated as follows, with I_1 and J_2 as the stress invariants and α and K being the material parameters [38].

$$f(I_1, J_2) = \alpha I_1 + \sqrt{J_2} - K = 0 . \qquad (7.13)$$

Suppose the material has a tensile yield strength of σ_t and compressive yield of σ_c ,then when subjected to a combination of normal stress σ and shear stress τ, there arises two cases.

Pure Tension

$$\boxed{\begin{aligned} I_1 &= \sigma_t \\ J_2 &= \frac{\sigma_t^{\,2}}{3} \end{aligned}}$$

Pure Compression

$$\boxed{\begin{aligned} I_1 &= -\sigma_c \\ J_2 &= \frac{\sigma_c^{\,2}}{3} \end{aligned}}$$

Imposing the tension and compression conditions on the functional form from Equation (7.13) gives

$$\alpha\sigma_t + \frac{\sigma_t}{\sqrt{3}} - K = 0 \text{ and} \tag{7.14}$$

$$-\alpha\sigma_c + \frac{\sigma_c}{\sqrt{3}} - K = 0\,. \tag{7.15}$$

Hence, for a stress state (σ,τ), the stress invariants I_1 and J_2 are given by

$I_1 = \sigma$, and

$J_2 = \frac{\sigma^2}{3} + \tau^2$.

Substituting for I_1 and J_2 in Equation (7.13), gives

$$f(\sigma,\tau) = \alpha\sigma + \sqrt{\frac{\sigma^2}{3} + \tau^2} - K = 0\ . \tag{7.16}$$

We attempt to eliminate the parameters by finding a set of equations that can be simultaneously solved numerically to give the values of α and K . That is, by applying pure tension and compression conditions in the governing equation of the Drucker - Prager yield criterion, the values of the constants α and K were obtained, i.e.,

$$\alpha\sigma_t + \frac{\sigma_t}{\sqrt{3}} - K = 0 \text{ and}$$

$$-\alpha\sigma_c + \frac{\sigma_c}{\sqrt{3}} - K = 0\,.$$

According to Lu and Ravichandran [39],

$$\frac{\sigma_c}{\sigma_t} \cong 1.053\ . \tag{7.17}$$

The values of α and K were found to be equal to 0.0148 and $0.5921\sigma_t$ respectively from Equations (7.14) and (7.15).

Using Equation (7.13), the failure condition for a given stress state can be written as

$$f(\sigma,\tau) = (0.0148)\sigma + \sqrt{\frac{\sigma^2}{3} + \tau^2} - 0.5921\sigma_t = 0\ . \tag{7.18}$$

For the compression case, the parameter K is obtained as:

$$K = \left(\alpha - \frac{1}{\sqrt{3}}\right)\sigma_c = -0.5625\sigma_c\ .$$

Using Equation (7.13), the failure condition for a purely compression case can be expressed as

$$f(\sigma,\tau) = -(0.0148)\sigma + \sqrt{\frac{\sigma^2}{3} + \tau^2} + 0.5625\sigma_c = 0. \tag{7.19}$$

In order to establish the relationship between normal stress σ and shear stress τ, the basic expressions for stress invariant I_1 and core pressure P_0 from Ref. [29] were considered:

$I_1 = \sigma = 3P_m = 2P_0$ and (7.20)

$$P_0 = \frac{\tau}{0.31}\ . \tag{7.21}$$

In the above equation, P_0 and P_m are the core pressure and mean pressure, respectively.

Using Equations (7.20) and (7.21),

$$I_1 = \sigma = \frac{2\tau}{0.31}\ . \tag{7.22}$$

Using Equations (7.19) and (7.22), the analytical expression for compressive yield of metallic glass was found to be

$$\sigma_c = \left(\frac{-3.761259}{0.5625}\right)\tau\ . \tag{7.23}$$

τ is replaced by τ_{max} in Equation (7.23), where τ_{max} (the maximum shear stress under the indenter) can be calculated using nanoindentation.

The expression for τ_{max} is given by $\tau_{max} = 0.31\left(\frac{6PE^{*2}}{\pi^3\left(D/2\right)^2}\right)^{\frac{1}{3}}$ as per Ref. [29].

7.1.2 Model Based on Mohr-Coulomb Criterion

The Mohr-Coulomb criterion is based on the assumption that the maximum shear stress is only a decisive measure of impending failure. The criterion considers the limiting shear stress τ (in a plane) to be a function of the normal shear stress σ in the same plane. That is, $|\tau| = f(\sigma)$, where $f(\sigma)$ is an experimentally determined function [38]. The failure would occur if the radius of the largest principal circle is tangent to the envelope curve $f(\sigma)$. In other words it allows for the effect of the mean stress or the hydrostatic stress. The simplest form of $f(\sigma)$, the Coulomb equation having a straight line envelope is given by

$$|\tau| = c - \sigma \tan\phi. \qquad (7.24)$$

Here c and ϕ are material constants determined from the experiment.

Using Equation (7.24) and for $\sigma_1 \geq \sigma_2 \geq \sigma_3$, the Mohr-Coulomb criterion can be written as

$$\frac{1}{2}(\sigma_1 - \sigma_2)\cos\phi = c - \left[\frac{1}{2}(\sigma_1 + \sigma_2) + \frac{\sigma_1 - \sigma_3}{2}\sin\phi\right]\tan\phi.$$

Rearranging the above equation gives

$$\sigma_1 \frac{1+\sin\phi}{2c\cos\phi} - \sigma_3 \frac{1-\sin\phi}{2c\cos\phi} = 1.$$

The tensile yield strength σ_t and compressive yield σ_c parameters are defined as follows:

$$\sigma_c = \frac{2c\cos\phi}{1-\sin\phi}$$

and

$$\sigma_t = \frac{2c\cos\phi}{1+\sin\phi}\ ,$$

When the material is subjected to a combination of normal stress σ and shear stress τ, the yield criterion in terms of principal stresses and yield stresses is given as in Ref. [38],

$$\frac{\sigma_1}{\sigma_t} - \frac{\sigma_3}{\sigma_c} = 1 \qquad \sigma_1 \geq \sigma_2 \geq \sigma_3, \tag{7.25}$$

where σ_1 and σ_3 are given by

$$\sigma_1 = \frac{\sigma + \sqrt{\sigma^2 + 4\tau^2}}{2}, \text{ and}$$

$$\sigma_3 = \frac{\sigma - \sqrt{\sigma^2 + 4\tau^2}}{2}.$$

Substituting for σ_1 and σ_3 in Equation (7.25) gives

$$\frac{\sigma + \sqrt{\sigma^2 + 4\tau^2}}{2\sigma_t} - \frac{\sigma - \sqrt{\sigma^2 + 4\tau^2}}{2\sigma_c} = 1. \tag{7.26}$$

By using Equation (7.17) and substituting for σ_t in terms of σ_c in Equation (7.26), the failure condition for pure compression case was found to be,

$$(1.053)\frac{\sigma + \sqrt{\sigma^2 + 4\tau^2}}{2} - \frac{\sigma - \sqrt{\sigma^2 + 4\tau^2}}{2} = \sigma_c \tag{7.27}$$

Using Equations (7.22) and (7.27), the compressive yield stress based on the Mohr-Coulomb criterion can be written as

$$\sigma_c = \frac{14.2088}{2}\tau .$$

By replacing τ_{max} for τ, we get the yield stress under compression, where τ_{max} (the shear stress under the indenter) was determined from nanoindentation. The expression for τ_{max} is given in Equation (3.4).

7.2 Zr-based Bulk Metallic Glass

The Zr-based BMG was indented using spherical indenters of diameter 100 μm and 2.8 mm. All of the experiments yielded reproducible data as seen from the load-depth curves in the preceding chapter. The elastic modulus of the Zr-based BMG subjected to spherical indentation was obtained by fitting a 3/2 curve to the initial elastic portion of loading curve. Figure 7-1 shows a 3/2 fit to the initial elastic portion of the loading curve that followed the Hertzian law mentioned earlier. The elastic modulus was found to be 101 $\pm$ 5 GPa corresponding to experiment set A1 (Figure 6-1). This agrees with the values reported in the literature [3].

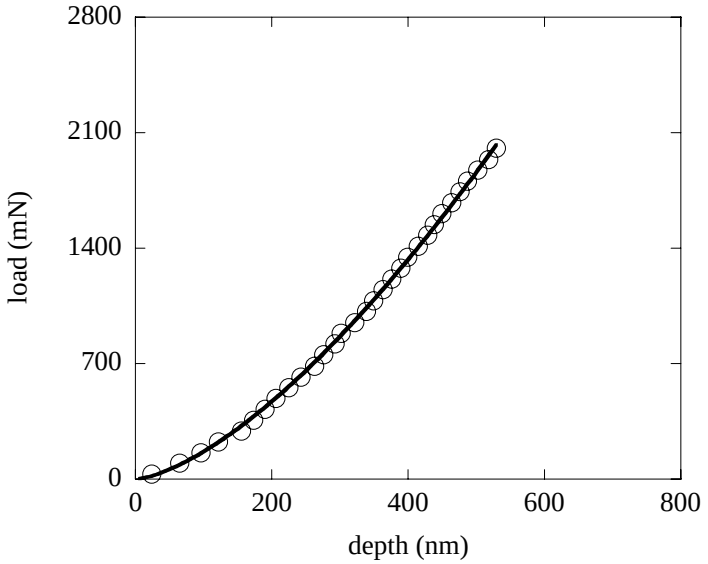

Figure 7-1: 3/2 fit to the initial elastic portion of the loading curve obtained by indenting Vitreloy 1 using a 2.8 mm diameter diamond spherical indenter.

Nanoindentation response of Vitreloy 1 using a 100 μm indenter corresponding to experiment set A2 yielded reproducible results. The modulus was found to be 95 $\pm$ 4 GPa. This agrees with the values reported in the literature [3]. As is evident the elastic modulus did not depend on the diameter of the indenter used indicative of the lack of residual stresses in the sample. As expected, being a relatively sharper indenter, the 100 μm diamond indenter produced large-scale plastic deformation, clearly because of the higher stress fields beneath the indenter. The choice of indenter diameter controlled the location of the maximum stress below the indenter as shown in Figure 7-2. As the diameter of the indenter increases, the stress value beneath the indenter decreases and the deformation tends to be more elastic in nature. This is evident in the load-depth measurements obtained by using indenters of different diameters.

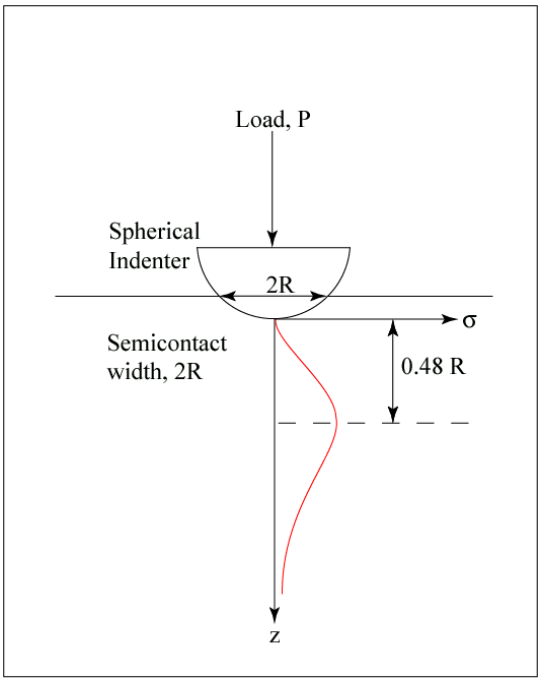

Figure 7-2: A schematic showing the location of maximum shear stress.

As per the Hertzian formulation, elastic contact is described by,

$$P = Ch^{\frac{3}{2}}$$

Taking log on both sides of the Hertzian formulation gives

$$\log\frac{P}{C} = \left(\frac{3}{2}\right)\log(h) \qquad (7.28)$$

As evident from Equation (7.28), on a log scale, the load-depth response of a material (that followed above-mentioned Hertzian law) follows a 3/2 slope. Any deviation from this slope of 3/2 on a log load vs. log depth plot indicates a deviation from the elastic behavior which is believed to be the onset of plastic deformation. The log scale analysis for the

calculation of the maximum shear stress under the indenter at the point of deviation as shown in Figure 7-3, yielded a value of 4.3 GPa for the compressive yield strength of Vitreloy 1. As is evident the yield strength value is much higher than the reported value for BMGs (~ 2 GPa). Hence it is believed that the first signs of plastic deformation occur at much lower loads than that can be detected from these logarithmic plots (Figure 7-3) and probably occurs as discrete bursts at lower loads.

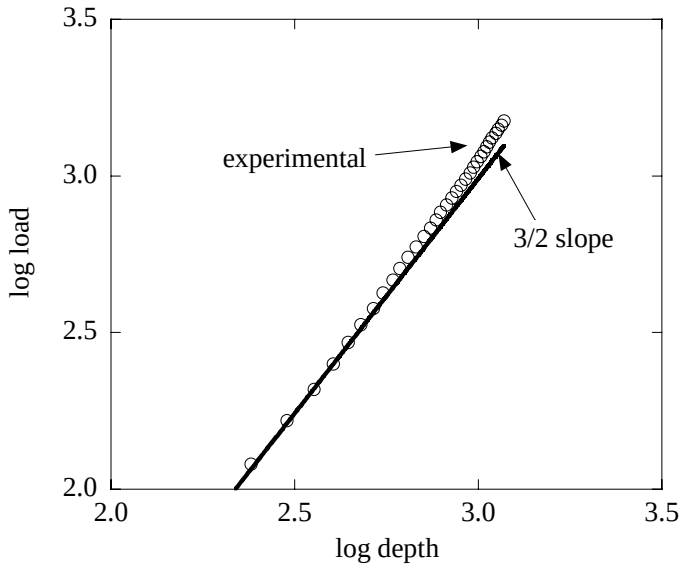

Figure 7-3: Log load vs. Log depth (loading portion) showing deviation from elastic behavior obtained by indenting Vitreloy 1 using a 100 μm indenter (corresponding to experiment set A2).

Figure 7-3 shows a portion of the load-depth response of Vitreloy 1 indented with a 100 μm indenter (experiment set A4), where the pop-in is likely associated with the shear band activity. By conducting experiment set A4, the discrete plastic events or "pop-ins" were captured. Attempts were made to correlate the initial pop-in events with the von Mises criterion and the analytical model to predict the yield strength of metallic glass. The yield stress corresponding to the initial plastic events, calculated based on von Mises criterion are tabulated in Table 7-1.

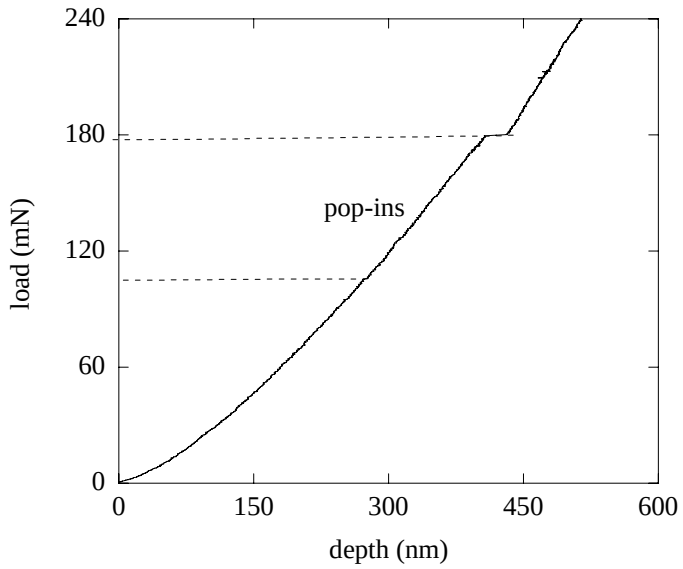

Figure 7-4: A portion of loading portion of the load-depth response of Vitreloy 1 obtained by indenting using a 100 μm indenter (corresponding to experiment set A3), where the pop-in is likely associated with shear band activity.

Table 7-1: The yield stress value corresponding to the initial set of discrete plastic events obtained from indenting Vitreloy 1 using a 100 μm indenter (experiment set A3), calculated based on the von Mises criterion.

Load where initial pop-in has occurred (mN)	Corresponding maximum shear stress under the indenter (MPa)	Yield stress von Mises Criterion (GPa)
105	116	2.32
179	133	2.66

The von Mises predictions were found to be close to the published yield strength value (~ 2GPa) indicating that the bursts were real and not an instrument artifact. The analytical models based on the Drucker-Prager and the Mohr-Coulomb criterion predicted an unrealistically large value of around 8 GPa and 9 GPa, respectively, for the yield strength of Vitreloy 1. The discrepancy in the models and the von Mises prediction (Table 7-1) could be attributed to the error in the core pressure P_0 and σ_c/σ_t relationships and the sensitivity of these values considered in the model. To check if the discrete bursts seen in the case of Zr-based BMG were characteristic of the material, the standard material (fused quartz) was indented under similar experimental conditions (experiment set A3). Nanoindentation experiments of fused quartz showed no discrete bursts under similar experimental conditions (Figure 7-5) illustrating that the discrete burst was indeed a material specific event and not an instrument artifact.

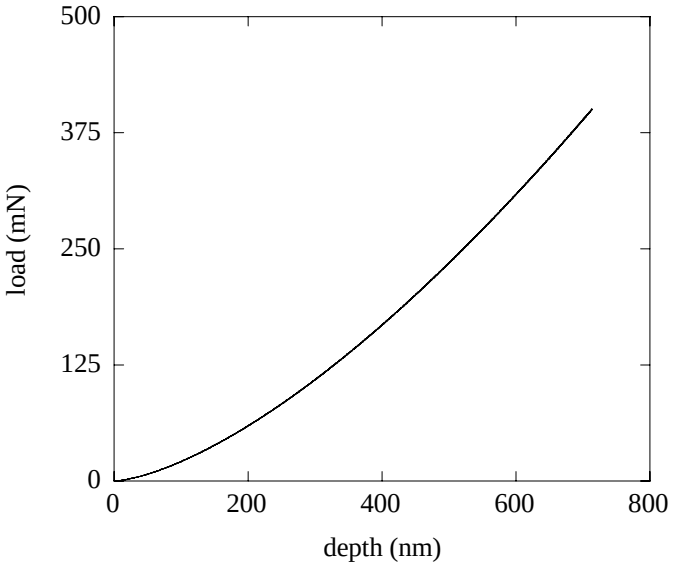

Figure 7-5: Load-depth response of fused quartz indented using a 100 μm indenter, with experiments conditions (experiment set A3) showing absence of pop-in events.

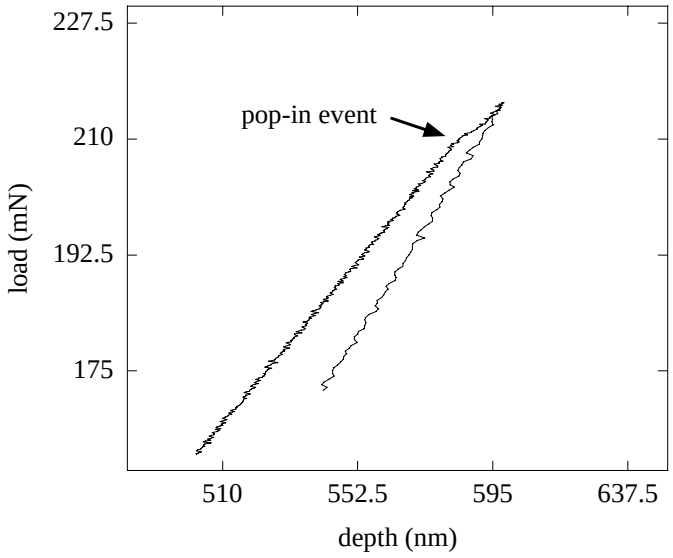

Figure 7-6: Nanoindentation response of Vitreloy 1 corresponding to the fifth iteration in the multiple cycle loading experiments using a 100 μm indenter (experiment set A4)

Figure 7-6 shows the fifth iteration in the multiple cycle loading experiments with the partial unloading portion of the curve very close to the discrete burst. Nanoindentation experiments of multiple load cycles with increasing loads (10 % unload) showed a change in slope immediately after the displacement burst had occurred (Figure 7-6) illustrating how a displacement burst influenced the load-depth response and how shear bands affected the subsequent deformation response. As observed in Figure 7-6, the slope change was very rapid. A gradual change in slope was observed by increasing the number of cycles in the experiment set A4 from 8 to 21 cycles (Figure 6-6).

7.3 Cu-based Bulk Metallic Glass

Investigations into the deformation characteristics of Cu-based BMG samples using instrumented indentation yielded the load-depth response presented in the preceding chapter. Porosity was observed in the sample during the sample preparation for indentation. As a result, severe contact problems were encountered while using 2.0 mm and 2.8 mm diameter diamond spherical indenters.

The elastic modulus of the Cu-based BMG subjected to spherical indentation was obtained from its load-depth response. Figure 7-7 shows a 3/2 fit to the initial elastic portion of the loading curve that followed the Hertzian law mentioned earlier.

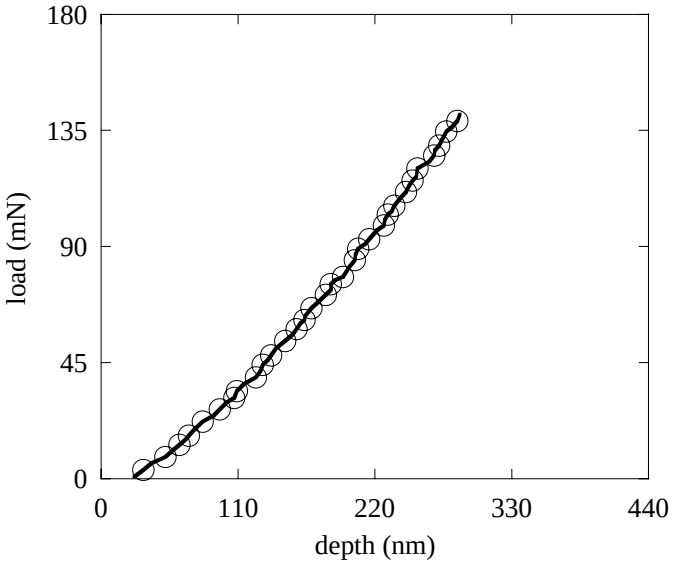

Figure 7-7: 3/2 fit to the elastic portion of the loading curve obtained by indenting $Cu_{60}Hf_{25}Ti_{15}$ using a 100 μm diamond spherical indenter.

Analysis of the data in a manner similar to the procedure adopted for Zr-based BMG (Chapter 5), resulted in an elastic modulus of 94 GPa for $Cu_{60}Hf_{25}Ti_{15}$ and 98 GPa for $Cu_{60}Zr_{30}Ti_{10}$ samples, respectively using a 100 μm diamond spherical indenter. The moduli were comparable to the values reported in literature (114 GPa for $Cu_{60}Zr_{30}Ti_{10}$ and 124 GPa for the $Cu_{60}Hf_{25}Ti_{15}$ alloys as per the compression tests [40]).

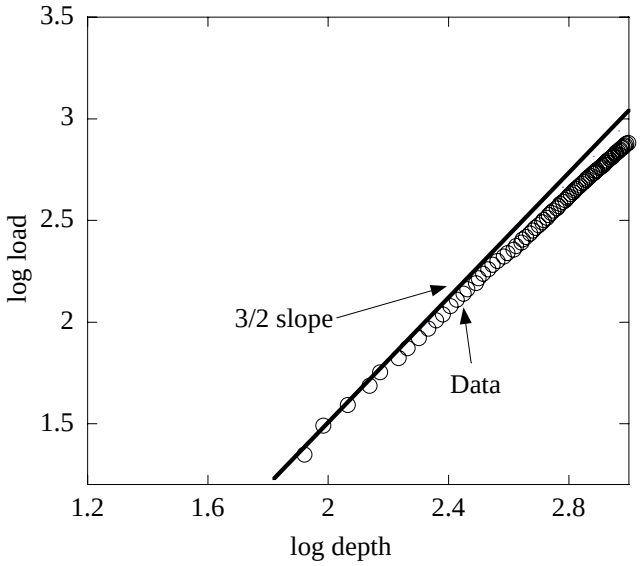

Figure 7-8: Log load vs. log depth plot showing deviation from 3/2 slope obtained by indenting using a 100 μm diamond spherical indenter.

Deviation from this slope of 3/2 on a log load vs. log depth plot indicated a deviation from elastic behavior (Figure 7-8). Hence the loading portion of the load-depth curve corresponding to experiment sets B1 and B2 were plotted on a log scale to determine the onset of large-scale plastic deformation. The values of maximum shear stress (using the analysis described earlier) were found to be 1.23 $\pm$ 0.20 GPa for $Cu_{60}Hf_{25}Ti_{15}$ and 1.13 $\pm$ 0.1 GPa for $Cu_{60}Zr_{30}Ti_{10}$ alloys respectively and the corresponding yield strength values were found to be 2130 MPa for $Cu_{60}Hf_{25}Ti_{15}$ and 1957 MPa for $Cu_{60}Zr_{30}Ti_{10}$ alloys.

The yield strength values were comparable to the values reported in literature (1785 MPa for the $Cu_{60}Zr_{30}Ti_{10}$ alloy and 2010 MPa for the $Cu_{60}Hf_{25}Ti_{15}$ alloy as per the compression tests [40]).

7.4 Fe-based Bulk Metallic Glass

The elastic modulus was determined to be 53 ± 15 GPa. There was too much of scatter in the data. The consolidation parameters used for HIPing and magnetic compaction of the BMG powder, are obviously not optimum to achieve 100 % density. Porosity could also be one of the reasons for scatter in the data. Optimization of the consolidation process of mechanically alloyed amorphous powders for full density is very essential for data reliability and reproducibility.

CHAPTER 8 : CONCLUSIONS AND FUTURE WORK

A methodology for using instrumented indentation at nano- and micro- scales to determine the mechanical response of bulk metallic glasses (BMGs) was developed and implemented. The implementation in Zr-, Cu- and Fe- based glasses primarily focused on deformation in the elastic regime but included preliminary results related to the onset of inelastic deformation.

Analytical formulations were developed for extracting the mechanical response from load- depth indentation results on the instrument's Nano and Micro Test Platforms. The methodology developed included calibration techniques, formulations to extract the contact compliances, verifications using standards and verification procedures for uniqueness of instrument deformation under a spherical indenter. The methodology was different for the two platforms based on the load - depth response characteristics of the instrument. The load - depth response of the instrument was linear in the case of the Micro Test platform. The load - depth response of the instrument was determined by subtracting the theoretical response from the corresponding raw load - depth response obtained by elastically indenting a standard steel specimen of known modulus (210 GPa). Consequently, the true response of the sample was obtained by subtracting the machine's response from the corresponding uncorrected load-depth response (raw data). As an added check, the instrument compliance determined by indenting steel was used to determine the modulus of a standard quartz sample and values obtained were within error limits of the standard. On the Nano Test platform, the instrument deformation displayed considerable elastic recovery that followed a 3/2 power law. This posed

a challenge in obtaining valid mechanical property data for characterizing the materials using instrumented indentation at nano scales. There was no existing model to account for the instrument deformation. Formulations to extract the contact compliances included proposing a new model to describe the load train. Initial attempts showed that the assumptions made in the formulation were not adequate to account for the response characteristics of the overall indentation response. The model was reformulated. Tungsten was used as a material standard for verifying the uniqueness of instrument deformation at nano scales. The methodology facilitated property extraction and consequently was extended to investigate the indentation response of BMGs.

Spherical diamond indenters of different diameters (2.8 mm and 100 μm) were used to probe both elastic and inelastic deformation in bulk metallic glasses of varying composition. The spherical geometry resulted in a simpler stress distribution under the indenter (when compared to a sharp geometry) but more importantly by resorting to spherical indenters the onset of plastic deformation was delayed. The experiments were conducted on Zr-, Cu- and Fe-based bulk metallic glasses.

In the case of the Zr-based BMG, the experiments showed that the elastic response did not depend on the diameter of the indenter used indicative of the lack of residual stresses in the sample. Large scale plastic deformation was observed when the sample was indented using a sharper indenter. Log scale analysis (i.e., examining the results on a log load vs. log depth response to check for deviation from Hertizian behavior) showed a deviation from 3/2 slope indicating a deviation from elastic behavior. The onset of deviation gave a yield strength value of 4 GPa, higher than the reported value in literature (~ 2 GPa). Hence it was believed that the

first signs of plastic deformation occurred at much lower loads than the predicted loads from the log scale analysis procedure and would probably occur as discrete bursts. Discrete plastic events or “pop-ins” were observed in the load-depth indentation responses under quasi static loading conditions, which were believed to be associated with shear band activity. An attempt was made to formulate a mathematical model based on two pressure sensitive yield criterions (Drucker-Prager and Mohr-Coulomb’s yield criterion) and the von Mises criterion that predicts the yield strength of metallic glasses. The predictions were partially correlated with the initial plastic events observed in the load-depth indentation responses. The predictions based on the von Mises criterion showed weak pressure sensitivity and yield strength values obtained were very close to the actual value (~ 2 GPa). The predictions based on the analytical model gave unrealistic numbers owing to the sensitivity associated with the mean pressure and ratio of compressive to tensile yield strength values. Based on the Mises predictions and comparable experiments on a quartz standard, it was established that the pop-ins were real and not an instrument artifact. Multiple load cycle following partial unload experiments showed that the pop-ins affected the subsequent indentation response.

The modulus values and the yield strength values obtained for the Cu-based BMG were comparable to the values reported in literature. There was too much of scatter in the indentation data of the Fe-based BMG. Porosity and lack of 100 % compaction were believed to be the reasons for scatter in the data.

Future work will be aimed at using spherical diamond indenters at multiple length scales to assess the effect of geometrical size scale associated with the evolution and interaction of shear bands and their subsequent propagation to the surface of the specimen in a systematic

manner. The influence of pre-introduced shear bands on the indentation response will also be investigated. The surface residual stress effects on indentation response will also be investigated based on Hertzian and Oliver Pharr approaches. The observations will be substantiated with microscopy and finite element modeling.

LIST OF REFERENCES

1. S. Rajagopalan and R. Vaidyanathan, J. Min. Met. Mat. S., 2002, **54**, p. 45.
2. A. Inoue, Acta. Mater., 2000, **48**, p. 279.
3. R. Vaidyanathan, M. Dao, G. Ravichandran, and S. Suresh, Acta. Mater., 2001, **49**, p. 3781.
4. A. C. Schuh and T. G. Nieh, Acta. Mater., 2003, **51**, p. 87.
5. W. L. Johnson, Mater. Res. Bull., 1999, p. 42.
6. S. Schneider, J. Phys.: Condens. Matter, 2001, **13**, p. 7723.
7. W. L. Johnson, Curr. Opin. Solid State Mater. Sci., 1996, **1**, p. 383.
8. W. H. Wang, C. Dong, and C. H. Shek, Materials Science and Engineering: R: Reports, 2004, **44**, p. 45.
9. J. F. Löffler, Intermetallics, 2003, **11**, p. 529.
10. A. Inoue, H. Yamaguchi, T. Zhang, and T. Masumoto, Mater. Trans., JIM, 1990, **31**, p. 104.
11. A. Peker and W. L. Johnson, Appl. Phys. Lett., 1993, **63**, p. 2342.
12. C. Fan, R. T. Ott, and T. C. Hufnagel, Appl. Phys. Lett., 2002, **81**, p. 1020.
13. W. J. Wright, T. C. Hufnagel, and W. D. Nix, J. Appl. Phys., 2003, **93**, p. 1432.
14. T. Mukai, T. G. Nieh, Y. Kawamura, A. Inoue, and K. Higashi, Scripta Mater., 2002, **46**, p. 43.
15. C. Tang, Y. Li, and K. Zeng, Materials Science and Engineering A, 2004, **384**, p. 215.
16. U. Ramamurty, S. Jana, Y. Kawamura, and K. Chattopadhyay, Acta. Mater., 2005, **53**, p. 705.
17. W. J. Wright, R. Saha, and W. D. Nix, Materials Transactions, 2001, **42**, p. 642.
18. T. Mukai, T. G. Nieh, Y. Kawamura, A. Inoue, and K. Higashi, Intermetallics, 2002, **10**, p. 1071.
19. Y. Leng and T. H. Courtney, J. Mater. Sci, 1991, **26**, p. 588.
20. A. V. Sergueeva, N. A. Mara, J. D. Kuntz, D. J. Branagan, and A. K. Mukherjee, Mat. Sci. Eng. A - Struct., 2004, **383**, p. 219.

21. L. F. Liu, L. H. Dai, Y. L. Bai, B. C. Wei, and J. Eckert, Mater. Chem. Phys., 2005, **93**, p. 174.
22. B. J. Edwards, K. Feigl, M. L. Morrison, B. Yang, P. K. Liaw, and R. A. Buchanan, Scripta Mater., 2005, **53**, p. 881.
23. T. C. Hufnagel and R. P. Vinci, Scripta Mater., 2000, **43**, p. 1071.
24. W. J. Wright, R. B. Schwarz, and W. D. Nix, Mat. Sci. Eng. A - Struct., 2001, p. 229.
25. B. P. Kanungo, C. S. Glade, A. K. Palakkal, and K. M. Flores, Intermetallics, 2004, **12**, p. 1073.
26. M. Telford, Mater. Today, 2004, **7**, p. 36.
27. A. C. Fischer-Cripps, *Nanoindentation*. 2002, New York: Springer-Verlag.
28. J Alcala, A. E. Giannakopoulos, and S. Suresh, Journal of Materials Research, 1998, **13**, p. 1390.
29. K. L. Johnson, *Contact Mechanics*. 1985, Cambridge: Cambridge University Press.
30. A. Schuh and T. Nieh, J. Mater. Res., 2004, **19**, p. 46.
31. M. N. M. Patnaik, R. Narasimhan, and U. Ramamurty, Acta. Mater., 2004, **52**, p. 3335.
32. A. L. Greer, A. Castellero, S. V. Madge, I. T. Walker, and J. R. Wilde, Mat. Sci. Eng. A - Struct., 2004, **375**, p. 1182.
33. A. C. Schuh, A. S. Argon, T. G. Nieh, and J. Wadsworth, Philos. Mag. A **83**, p. 2585.
34. C. Tang, Y. Li, and K. Zeng, Mater. Lett., 2005, **59**, p. 3325.
35. L. Liu and K. C. Chan, Mater. Lett., 2005, **59**, p. 3090.
36. L. Anand and C. Su, J. Mech. Phys. Solids, 2005, **53**, p. 1362.
37. B. Yang, L. Riester, and T. G. Nieh, Scripta Mater., 2006, **54**, p. 1277.
38. W. Chen and D. J. Han, *Plasticity for Structural Engineers*. 1988, New York: Springer Verlag.
39. J. Lu and G. Ravichandran, J. Mater. Res., 2003, **18**, p. 2039.
40. A. Inoue, W. Zhang, T. Zhang, and K. Kurosaka, Acta. Mater., 2001, **49**, p. 2645.